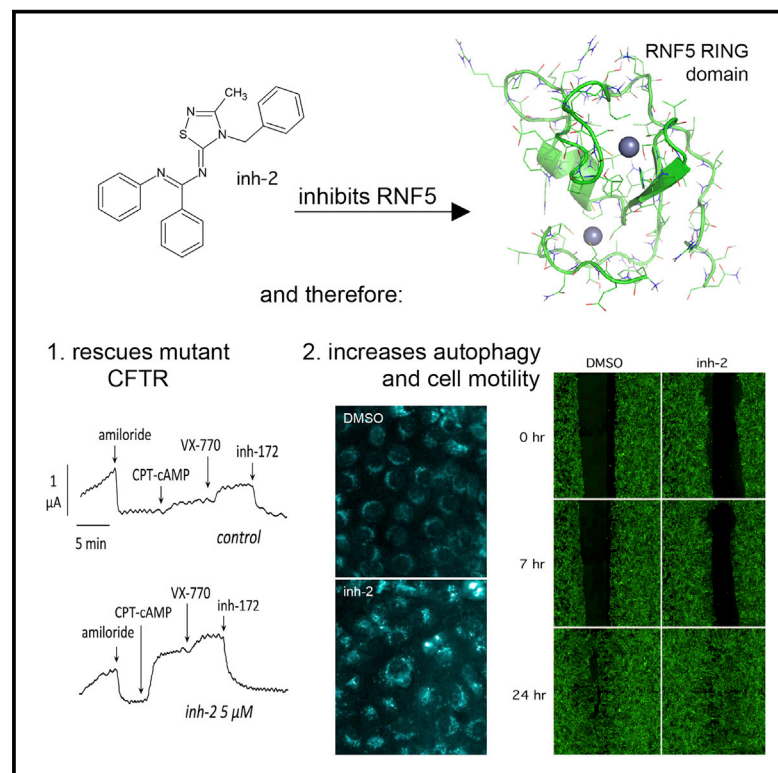


Cell Chemical Biology

Pharmacological Inhibition of the Ubiquitin Ligase RNF5 Rescues F508del-CFTR in Cystic Fibrosis Airway Epithelia

Graphical Abstract



Authors

Elvira Sondo, Federico Falchi, Emanuela Caci, ..., Roberto Ravazzolo, Andrea Cavalli, Nicoletta Pedemonte

Correspondence

andrea.cavalli@unibo.it (A.C.),
nicoletta.pedemonte@unige.it (N.P.)

In Brief

Sondo et al. used a computational approach to identify an inhibitor, named inh-02, for RNF5 ubiquitin ligase. RNF5 detects the misfolding of a mutant CFTR in cystic fibrosis. Inh-2 decreases ubiquitylation and rescues F508del-CFTR on human primary bronchial epithelia. This work validates RNF5 as a drug target for cystic fibrosis.

Highlights

- Homology modeling/virtual ligand screening identified RNF5 inhibitor inh-2
- Inh-2 rescues F508del-CFTR activity on human primary bronchial epithelia
- Inh-2 decreases ubiquitylation and increases half-life of F508del-CFTR
- Inh-2 modulates RNF5 downstream pathways

Pharmacological Inhibition of the Ubiquitin Ligase RNF5 Rescues F508del-CFTR in Cystic Fibrosis Airway Epithelia

Elvira Sondo,^{1,6} Federico Falchi,^{2,3,6} Emanuela Caci,¹ Loretta Ferrera,¹ Elisa Giacomini,³ Emanuela Pesce,¹ Valeria Tomati,¹ Sine Mandrup Bertozzi,⁴ Luca Goldoni,⁴ Andrea Armirotti,⁴ Roberto Ravazzolo,^{1,5} Andrea Cavalli,^{2,3,*} and Nicoletta Pedemonte^{1,7,*}

¹U.O.C. Genetica Medica, Istituto Giannina Gaslini, Via Gerolamo Gaslini 5, Genova 16147, Italy

²Dipartimento di Farmacia e Biotecnologie, University of Bologna Alma Mater Studiorum, Bologna 40126, Italy

³D3 Compunet, Fondazione Istituto Italiano di Tecnologia, Genova 16163, Italy

⁴Analytical Chemistry Facility, Fondazione Istituto Italiano di Tecnologia, Genova 16163, Italy

⁵DINOGMI Department, University of Genova, Genova 16132, Italy

⁶These authors contributed equally

⁷Lead Contact

*Correspondence: andrea.cavalli@unibo.it (A.C.), nicoletta.pedemonte@unige.it (N.P.)

<https://doi.org/10.1016/j.chembiol.2018.04.010>

SUMMARY

In cystic fibrosis (CF), deletion of phenylalanine 508 (F508del) in the CFTR channel is associated with misfolding and premature degradation of the mutant protein. Among the known proteins associated with F508del-CFTR processing, the ubiquitin ligase RNF5/RMA1 is particularly interesting. We previously demonstrated that genetic suppression of RNF5 *in vivo* leads to an attenuation of intestinal pathological phenotypes in CF mice, validating the relevance of RNF5 as a drug target for CF. Here, we used a computational approach, based on ligand docking and virtual screening, to discover inh-02, a drug-like small molecule that inhibits RNF5. In *in vitro* experiments, treatment with inh-02 modulated ATG4B and paxillin, both known RNF5 targets. In immortalized and primary bronchial epithelial cells derived from CF patients homozygous for the F508del mutation, long-term incubation with inh-02 caused significant F508del-CFTR rescue. This work validates RNF5 as a drug target for CF, providing evidence to support its druggability.

INTRODUCTION

Cystic fibrosis (CF) is the most frequent genetic disease in Caucasian populations (1 affected in every ~3,000 births). It is caused by loss-of-function mutations in the gene that encodes the CF transmembrane conductance regulator (CFTR). CFTR is a cAMP-regulated chloride channel expressed at the apical membrane of many types of epithelial cells. CF is a multi-organ disease, characterized by chronic lung infection and deterioration of lung function, pancreatic insufficiency, male infertility, and meconium ileus (Pilewski and Frizzell, 1999). The deletion

of phenylalanine 508 (F508del) is the most common CF mutation (~90% of all CF alleles). F508del-CFTR shows a misfolding defect, which leads to reduced stability and/or defective interactions between separate domains of the CFTR protein. The mutant channel is retained in the ER and prematurely degraded by the ubiquitin/proteasome system. Plasma membrane expression is thus reduced (trafficking defect) (Du et al., 2005). In addition, activity of the mutant channel is severely decreased due to a reduced open-channel probability (gating defect) (Dalemans et al., 1991).

Druggability of F508del-CFTR has been demonstrated by several studies. At present, two such molecules are commercially available for CF patients. Ivacaftor, previously known as VX-770, is a potentiator, i.e., a molecule that increases the activity of CFTR mutants with gating defects (Yu et al., 2012). A combination of ivacaftor plus lumacaftor, also known as VX-809, is the second drug that has been approved to treat CF patients homozygous for the F508del mutation. Lumacaftor is a corrector, i.e., a molecule that improves the maturation and trafficking of F508del-CFTR to the membrane (Wainwright et al., 2015).

Different mechanisms of action of correctors have been proposed. Correctors could act as pharmacological chaperones or as proteostasis regulators. Pharmacological chaperones act on mutant CFTR by stabilizing specific CFTR domains and/or by improving interactions of separate CFTR domains (Okuyoneda et al., 2013). Proteostasis regulators modulate the proteostasis environment, leading to beneficial effects on CFTR processing (Balch et al., 2008).

A single corrector is generally not considered sufficient to promote a therapeutically relevant F508del-CFTR rescue. Rather, CF drug therapy is thought to require more than one pharmacological chaperone or a combination with a proteostasis regulator. Novel drug targets and their modulators must therefore be identified in order to design new CF therapies. One of the most promising targets is the ubiquitin ligase RNF5/RMA1 (Tomati et al., 2015; Sondo et al., 2017). RNF5/RMA1 is an E3 ubiquitin ligase acting at early stages of CFTR biosynthesis, promoting its degradation (Younger et al., 2006). Recently, our group demonstrated

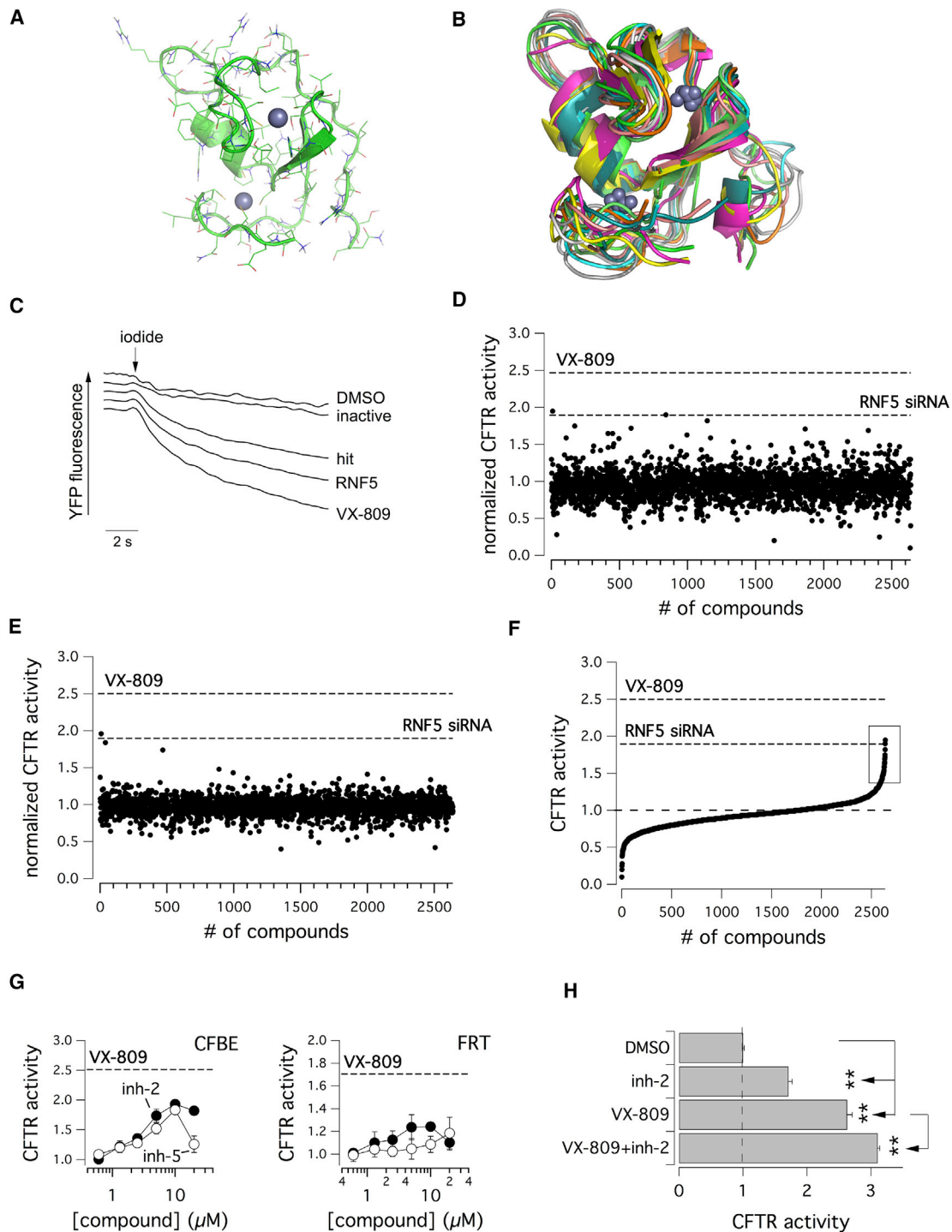


Figure 1. Generation of a Homology Model of RNF5 RING Domain for Ligand Docking Based Screening and Biological Evaluation of Putative RNF5 Inhibitors as Mutant CFTR Correctors

(A) Example of a single RNF5 conformation.

(B) Superimposition of the 10 RNF5 protein conformations selected for the virtual screening. The protein is represented as cartoon and line, the zinc ions as spheres. See also [Figure S1](#) and [Table S1](#).

(C) Representative traces of the YFP functional assay on CFBE410⁻ cells expressing F508del-CFTR.

(D and E) Results of the compound library screening performed on F508del-CFTR-expressing CFBE410⁻ cells, using the YFP functional assay. Each dot represents CFTR activity following treatment with a single compound at 10 μ M (D) or at 2 μ M (E).

(legend continued on next page)

that genetically suppressing the ubiquitin ligase RNF5/RMA1 *in vivo* attenuates the pathological phenotypes due to intestinal malabsorption in F508del/F508del mice, and concomitantly increases CFTR activity in intestinal epithelial cells (Tomati et al., 2015). This previous work validates RNF5 as a drug target for CF. However, to date, no RNF5 inhibitors have been reported.

Here, we used a computational approach, based on ligand docking and virtual screening, to discover inh-02, a drug-like small molecule that inhibits RNF5. Long-term incubation with inh-02 caused significant F508del-CFTR rescue in immortalized and primary bronchial epithelial cells from CF patients homozygous for the F508del mutation. We characterized inh-2's mechanism of action, confirming that it decreases ubiquitylation of mutant CFTR, causing stabilization of the mature form of CFTR. In addition, inh-2 acts on ATG4B and paxillin, which are known targets downstream of RNF5 (Didier et al., 2003; Kuang et al., 2012).

RESULTS

Homology Modeling and Virtual Ligand Screening to Identify RNF5 Inhibitors

From a computational standpoint, human RNF5 is a very challenging target. To date, there are no structures available in the PDB, and no known inhibitors. Moreover, there is very low identity with similar proteins in the PDB for homology modeling endeavors. Therefore, we used two complementary approaches to identify potential RNF5 inhibitors. First, we used homology modeling to build the 3D structure of RNF5. We started from the RNF5 sequence downloaded from the UniProt, and from a list of potential templates (Table S1) with identity between 28% and 42%. After 250 ns of molecular dynamics (MD) simulations, 10 protein conformations were clustered and eventually retained (Figure 1). Then, the ten conformations were submitted to druggability tests to identify suitable pockets for virtual ligand screening. All the ligands from the Life Chemicals database (about 500K) were docked into these pockets with GLIDE (SP scoring function). The 1,000 top-scoring compounds for each protein conformation were stored. The selected compounds (10,000) were visually inspected and clustered. A total of 1,623 suitable compounds were identified. To obtain more chances of success of the virtual screening, a second and complementary approach was used. We built a diversity set of 1,000 compounds to obtain the most diverse compounds that span the entire descriptor space of the LifeChemicals database, using the Canvans software on the basis of the MOLPRINT 2D fingerprints. Finally, 2,623 molecules were purchased and biologically tested.

Biological Evaluation of Test Compounds as F508del-CFTR Correctors

As a primary screen, we tested the compounds for their ability to rescue the F508del-CFTR trafficking defect in CFBE41o⁻ bronchial epithelial cells, stably co-expressing F508del-CFTR and the halide-sensitive yellow fluorescent protein (HS-YFP). This

cell line has been extensively used by our group, in combination with the microfluorimetric assay based on the HS-YFP, to identify and characterize various CFTR rescue maneuvers, including proteostasis regulators (Pedemonte et al., 2011; Sondo et al., 2011; Pesce et al., 2015, 2016; Tomati et al., 2015, 2018). Twenty-four hours after plating, cells were treated with test compounds (2- and 10- μ M final nominal concentration). The vehicle alone (DMSO) and corrector VX-809 (1 μ M) were used as negative and positive controls, respectively. In parallel, we also transfected cells with small interfering RNA (siRNA) molecules targeting RNF5. After an additional 24 hr, we assessed F508del-CFTR activity in the plasma membrane by measuring the rate of HS-YFP quenching caused by iodide influx into cells (Figure 1C). For each compound, we evaluated the resulting CFTR activity, normalized to the activity measured in negative controls. Results of the screenings are displayed in Figures 1D and 1E. CFTR activity scores (from the screening performed at 10 μ M) were then put into an ordered distribution (Figure 1F). Given the high reproducibility and robustness of the assay, we set an activity threshold of 1.4. Thus, compounds were considered active when CFTR activity was 40% higher than the control. The primary screening highlighted 43 putative hits, i.e., compounds able to elicit significant F508del-CFTR rescue and increased anion transport based on assessment of HS-YFP quenching, similar to what was observed following silencing of RNF5 with siRNA molecules (90%–95% increase in F508del-CFTR function over negative control cells). We used the YFP functional assay on F508del-CFTR CFBE41o⁻ cells to test the compounds at different concentrations. Surprisingly, we observed an extremely low hit-confirmation rate, with only two compounds having a clear dose-dependent effect. We named these compounds inh-2 and inh-5 (Figure 1G, left panel). The 50% effective concentration (EC₅₀) values for the two compounds were equal to 2.6 μ M for inh-2 and 3.4 μ M for inh-5. Very narrow dose-response curves were obtained for the other hits. These other compounds were active at only one or two concentrations, and showed marked cytotoxic effects at higher concentrations. To evaluate the possible effects of cell background on the activity of the hits, we tested the compounds at increasing concentrations on another cell model, Fischer rat thyroid (FRT) cells stably expressing F508del-CFTR and the HS-YFP (Figure 1G, right panel). The results showed that only inh-2 had a clear dose-dependent effect, with an EC₅₀ equal to 2.2 μ M, comparable to that obtained on CFBE41o⁻ cells. According to previous results from our group (Tomati et al., 2015) RNF5 suppression displayed an additive effect with VX-809. Thus, we evaluated mutant CFTR rescue in CFBE41o⁻ cells treated with inh-2 and VX-809 (alone and combined together) and we found that the two rescue maneuvers were additive (Figure 1H).

Compounds were bought in larger quantities (LifeChemical) and analyzed by NMR to confirm their chemical structures (Figure 2A). In parallel, inh-2 was also re-synthesized in house. During the synthesis, we observed the formation of a small amount of an undesired byproduct (roughly 10% compared with inh-2). This compound was a structural analog of inh-2

(F) Ordered distribution of the CFTR activity scores displayed in (C).

(G) Dose-response relationships using the YFP assay on CFBE41o⁻ and FRT cells.

(H) Additivity of inh-2 and VX-809 in F508del-CFTR CFBE41o⁻ cells (YFP assay).

Data are expressed as means \pm SEM, n = 4–6. Symbols indicate statistical significance versus control: **p < 0.01.

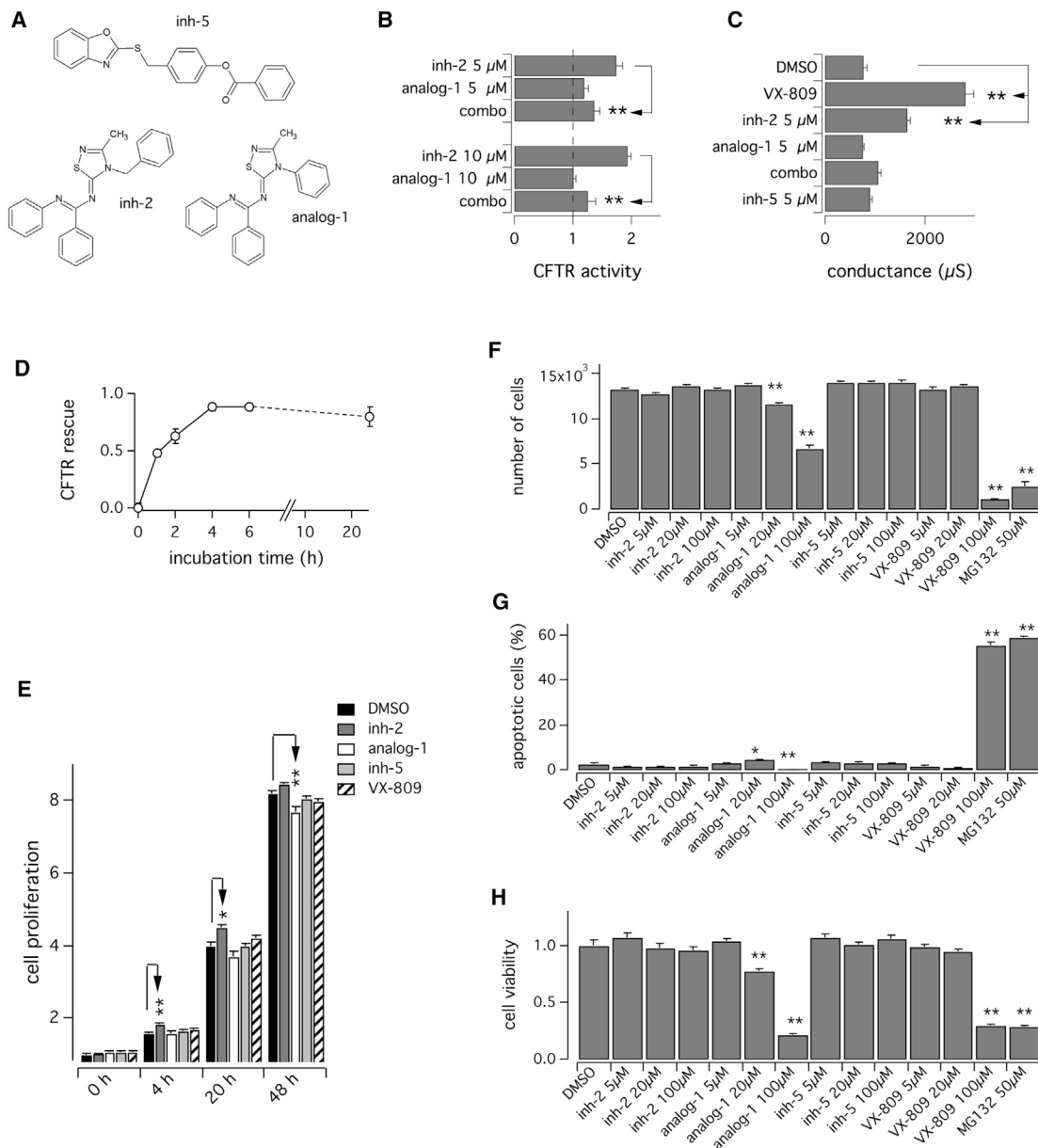


Figure 2. Validation of the F508del-CFTR Corrector Activity of the Putative RNF5 Inhibitors Derived from Primary Screening

(A) Chemical structures of selected hits and analog-1.

(B) F508del-CFTR activity measured on CFBE41o⁻ cells, using the YFP assay after 24 hr treatment with inh-2 and analog-1 alone and in combination (combo). Activity was normalized for the activity in DMSO-treated cells.

(C) Transepithelial electrical resistance measurements performed on F508del-CFTR-expressing FRT cells treated with indicated compounds. The bar graph shows the delta between the values of electrical resistance measured before and after CFTR inhibition, converted into its reciprocal conductance.

(D) Time course of CFTR rescue by inh-2. CFBE41o⁻ cells were incubated for different times with inh-2 (5 μM) at 37°C. F508del-CFTR activity was measured using the YFP assay.

(E) Bar graph showing the effect of test compounds (inh-2, analog-1, and inh-5: 5 μM; VX-809: 1 μM) on proliferation of CFBE41o⁻ cells.

(F and G) Bar graphs showing the number of living (F) and apoptotic (G) CFBE41o⁻ cells following 24 hr treatment with indicated compounds.

(H) CFBE41o⁻ cell viability as determined by the MTT cytotoxicity assay. Data are expressed as means ± SEM, n = 4–6. Symbols indicate statistical significance versus control: **p < 0.01, *p < 0.05.

(named analog-1). This compound was separated, purified, and collected for further evaluation (Figure 2A).

F508del-CFTR corrector activity of analog-1 was analyzed in CFBE41o⁻ cells (by measuring YFP quenching) and compared

with the activity of original hit inh-2. Analog-1 had no F508del-CFTR corrector activity. In addition, by combining analog-1 and inh-2, we observed that inh-2's ability to rescue mutant CFTR was severely decreased in the presence of its analog

(Figure 2B). To further evaluate the ability of these compounds to rescue F508del-CFTR, we performed transepithelial electrical resistance measurements, using FRT cells stably expressing F508del-CFTR. FRT cells were grown on permeable supports until they developed into tight epithelia. FRT epithelia were treated for 24 hr with test compounds or vehicle alone (DMSO) and then assayed. Transepithelial electrical resistance was measured for each epithelium before and after acute stimulation with forskolin (20 μ M) plus genistein (50 μ M) to fully activate CFTR. It was then measured after addition of the selective CFTR inhibitor PPQ-102 (30 μ M; see Tradtrantip et al., 2009) to completely block CFTR activity. The delta between the values of electrical resistance before and after CFTR inhibition was then converted into its reciprocal conductance and graphed in Figure 2C. In agreement with the results obtained using the YFP assay on FRT and CFBE41o⁻ cells, F508del-CFTR rescue by inh-2 significantly increased the transepithelial conductance. In contrast, epithelia treated with inh-5, analog-1, or the combination of analog-1 plus inh-2 displayed a conductance similar to that measured in negative controls (Figure 2C).

The time course of F508del-CFTR correction by inh-2 was analyzed in CFBE41o⁻ cells (by measuring YFP quenching) at different time points. F508del-CFTR correction was seen as early as 1 hr after compound addition, with maximal effect after 4–6 hr (Figure 2D).

Effect of Putative RNF5 Inhibitors on Cell Proliferation, Viability, and Apoptosis

We then evaluated first the effect of chronic treatment with test compounds (at the concentration tested for corrector activity) on the proliferation of CFBE41o⁻ cells. Therefore we plated YFP-expressing CFBE41o⁻ cells and evaluated cell proliferation for 48 hr following treatment with test compounds or vehicle alone (DMSO). Treatment with inh-2 caused a modest but statistically significant increase in cell proliferation at 4 hr and 20 hr after plating, without preventing cells from reaching confluency (Figure 2E). Conversely, cells treated with analog-1 showed a decreased proliferation at 48 hr after plating (Figure 2E). We then evaluated the effect of chronic treatment with high concentrations of test compounds on the proliferation and apoptosis of CFBE41o⁻ cells. Cell nuclei were counterstained with Hoechst 33342 and propidium iodide to visualize total and apoptotic cell count, respectively (Figures 2F and 2G). Long-term treatment with analog-1 (20 and 100 μ M) caused a significant decrease in cell proliferation, and an increase in the number of apoptotic cells, as compared with control condition (Figures 2F and 2G). Similar effect was observed upon treatment with VX-809 (100 μ M). Finally, we performed the cell viability assay based on the metabolic conversion of the 3-(4,5-dimethylthiazol-2-yl)-2,5-diphenyltetrazolium bromide (MTT) into a purple-colored formazan product (Figure 2H). The MTT assay highlighted a cytotoxic effect of incubation for 24 hr with analog-1 (20 and 100 μ M) as well as of VX-809 (100 μ M) (Figure 2H).

Putative RNF5 Inhibitor inh-2 Rescues F508del-CFTR Activity on Human Primary Bronchial Epithelia Derived from CF Patients

The ability of inh-2 to rescue F508del-CFTR was assayed on well-differentiated primary cultures of human bronchial epithelial

cells from four F508del homozygous subjects, using two different electrophysiological techniques: the transepithelial electrical resistance and potential difference measurements, and short-circuit current recordings in Ussing chamber (Figure 3). Bronchial epithelia were then treated for 24 hr with DMSO, or with inh-2, analog-1, or inh-5 (each compound at 5 μ M) or with the combination of inh-2 and analog-1. Epithelia were then assayed. Transepithelial electrical resistance and potential difference were measured for each epithelium before and after addition of amiloride (10 μ M) to block ENaC-mediated sodium absorption. They were then measured after full CFTR activation with forskolin (20 μ M) plus genistein (50 μ M). Finally, they were measured after CFTR inhibition due to addition of PPQ-102 (30 μ M). From the values of transepithelial resistance and potential difference measured before and after CFTR inhibition, we calculated the CFTR-dependent transepithelial conductance and equivalent short-circuit current for each condition (Figure 3A). Long-term treatment of CF primary bronchial epithelia with inh-2 significantly increased both CFTR-mediated conductance and equivalent short-circuit current. Disappointingly, no additivity was observed upon co-treatment with inh-2 and VX-809. Corrector activity of inh-2 was completely stopped by co-incubation with analog-1. Epithelia treated with inh-5 displayed CFTR-dependent activity non-significantly different from that of DMSO-treated epithelia (Figure 3A). Considering that F508del-CFTR rescue by inh-2 reached a maximal effect after 4–6 hr in CFBE41o⁻ cells (Figure 2D), we tested whether inh-2 and inh-5 could be effective in human bronchial epithelia upon 6 hr treatment. However, no significant rescue was detected under this condition (Figure 3A).

In parallel, F508del-CFTR homozygous bronchial epithelia were incubated for 24 hr with inh-2 or inh-5 (5 μ M) and with vehicle alone (DMSO). Epithelia were mounted in Ussing chambers to measure chloride secretion by short-circuit current analysis (Figure 3B). After blocking Na⁺ current with amiloride, cells treated with DMSO showed little response to the membrane-permeable cAMP analog CPT-cAMP, VX-770, or to selective CFTRinh-172 (Ma et al., 2002). Incubation with VX-809 for 24 hr resulted in the appearance of significant chloride current, as seen by the increased current after CPT-cAMP and VX-770, and inhibition by CFTRinh-172. Incubation with inh-2 for 24 hr increased chloride current, although to a lesser extent than VX-809 (Figure 3B). Epithelia co-treated with inh-2 and VX-809 displayed CFTR-dependent activity non-significantly different from that of VX-809 alone (Figure 3B). Epithelia treated with inh-5 displayed CFTR-mediated Cl⁻ secretion, which was not significantly increased over DMSO-treated epithelia (not shown).

Putative RNF5 Inhibitor inh-2 Decreases Ubiquitylation of F508del-CFTR thus Increasing its Half-Life in Immortalized Bronchial Epithelial Cells

It has been demonstrated that RNF5 acts at early stages of CFTR biosynthesis, promoting its ubiquitylation and therefore its degradation through the proteasome (Younger et al., 2006). Thus, we evaluated ubiquitylation of mutant CFTR in CFBE41o⁻ cells following 24 hr treatment with DMSO (vehicle), inh-2, inh-5, and VX-809 (Figure 4A). Subsequently, cells were treated for 4 hr with DMSO alone or with MG-132 (10 μ M; to block proteasomal degradation) and then lysed. Cell lysates were

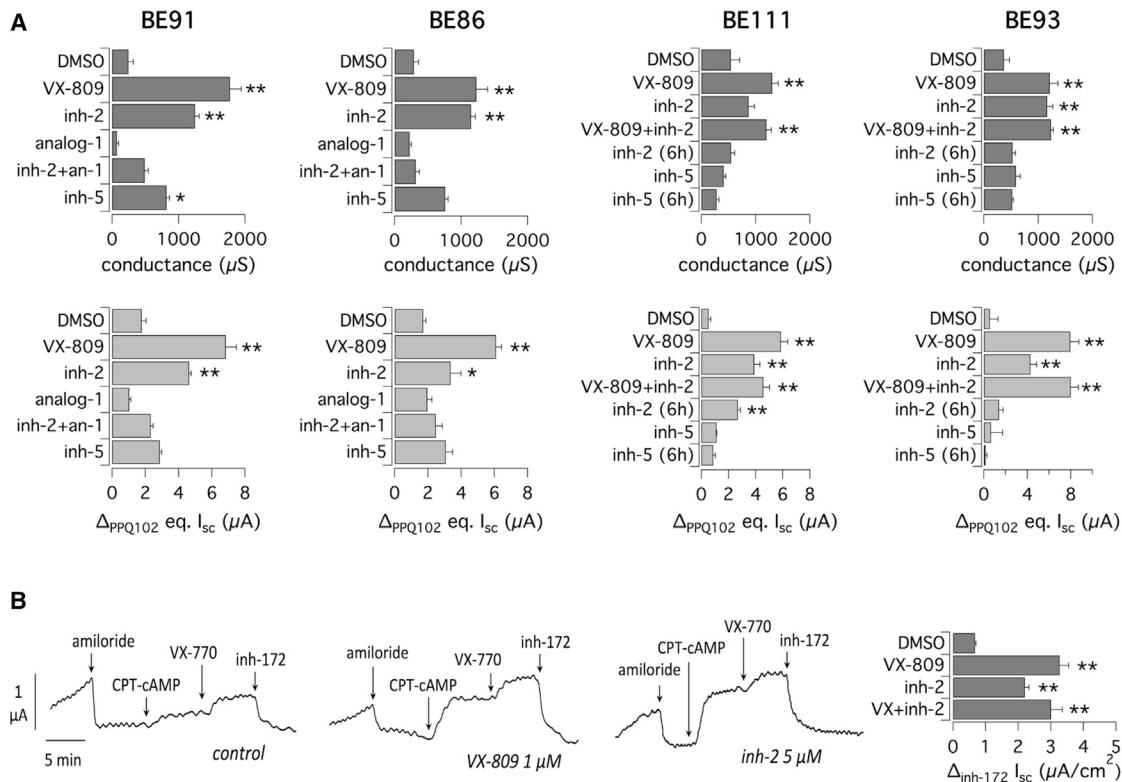


Figure 3. Correction of F508del-CFTR Activity in Human Primary Bronchial Epithelia by inh-2

(A) Transepithelial electrical resistance measurements performed on human primary bronchial epithelia derived from four different CF patients homozygous for the F508del mutation. Epithelia were treated for 24 hr (or 6 hr) with test compounds: inh-2 (5 μM), inh-5 (5 μM), analog-1 (an-1; 5 μM), VX-809 (1 μM), and VX-809 plus inh-2. The bar graphs show the delta between the values of electrical resistance measured before and after CFTR inhibition, converted into its reciprocal conductance (upper panels), and the equivalent short-circuit current (lower panels).

(B) Representative traces and bar graphs summarizing data (means \pm SEM) from the Ussing chamber recordings of human primary bronchial epithelia from a homozygous F508del patient (BE91), treated with inh-2 (5 μM), VX-809 (1 μM), and VX-809 plus inh-2 (VX + inh-2). Symbols indicate statistical significance versus control: ** $p < 0.01$, * $p < 0.05$.

immunoprecipitated using an anti-CFTR antibody and then subjected to SDS-PAGE followed by western blotting to evaluate CFTR expression and ubiquitylation status (Figures 4A–4D). The three test compounds rescued mutant CFTR, as shown by the appearance of the mature form of CFTR (band C; Figure 4A, CFTR blot), and evidenced also by the analysis of intensity profiles (Figure 4B). Treatment with MG-132 caused the appearance of CFTR forms at high molecular weight (at 250–300 kDa) that increased in the presence of test compounds, as evidenced by the analysis of intensity profiles (Figure 4C). Similarly, MG-132 caused the accumulation of ubiquitylated CFTR, particularly abundant in the absence of rescue maneuvers (Figure 4A, Ub blot), and decreased upon treatment with RNF5 inhibitors or VX-809 (Figures 4A and 4D), demonstrating that both the RNF5 inhibitors and VX-809 decreases ubiquitylation of mutant CFTR in CFBE41o⁻ cells.

We then evaluated the degradation rate of mutant CFTR in the absence or in presence of inh-2 and VX-809, alone or combined together. To this aim, we treated F508del-CFTR CFBE41o⁻ cells with test compounds and, after 24 hr, we blocked protein synthesis by adding cycloheximide to the medium. We then lysed cells at different time points, and cell lysates were subjected to

SDS-PAGE followed by western blotting to evaluate CFTR expression (Figure 4E). As shown in Figures 4E and 4F, the expression of mutant CFTR (both band B and C) decreases over time. However, when cells were treated with VX-809, the half-life of the mature form of mutant CFTR was significantly prolonged by 3-fold (from 1.25 to 4 hr; Figure 4F). Treatment with inh-2 alone was less effective than VX-809, causing a modest 50% increase in mature CFTR half-life (from 1.25 to 1.8 hr; Figure 4F). Interestingly, when cells were co-treated with VX-809 and inh-2, the half-life was further extended up to 6 hr (Figure 4F).

Evaluation of the Effect of RNF5 Inhibitors on RNF5 Downstream Pathways

Our data were obtained in a bronchial epithelial cell line and validated in human primary bronchial epithelia. They indicated that putative RNF5 inhibitors may indeed be an important therapeutic tool for rescuing F508del-CFTR. We thus sought to confirm the putative mechanism of action by investigating the effects of long-term treatment with inh-2 and analog-1 on RNF5-associated cellular readouts. ATG4B is one of the known targets of RNF5. Its ubiquitylation is mediated (at least partially) by RNF5 ligase activity (Kuang et al., 2012). We therefore performed *in vivo*

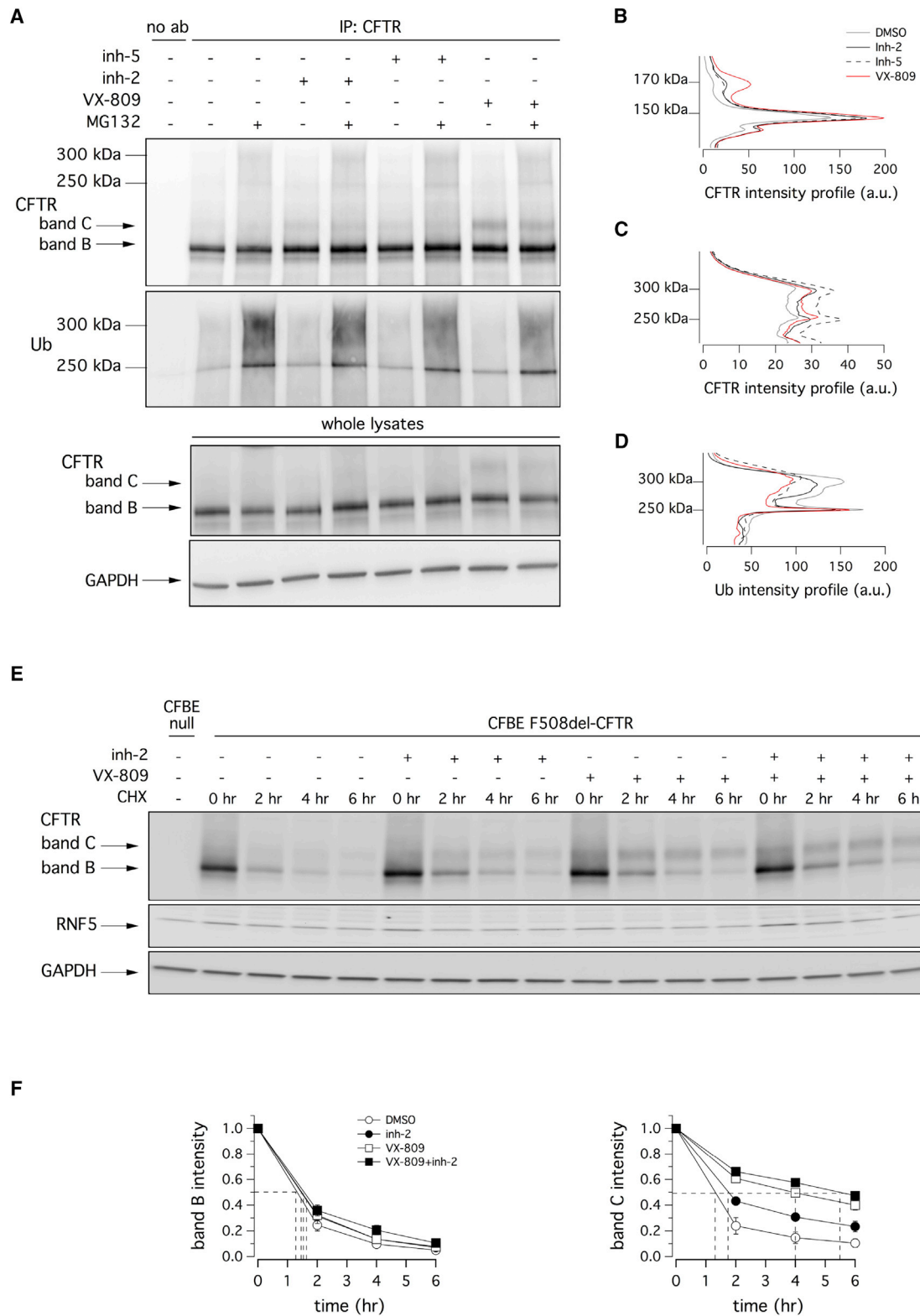


Figure 4. Reduced Ubiquitylation and Increased Half-Life of Mutant CFTR by RNF5 Inhibitors

(A) Biochemical analysis of CFTR ubiquitylation and expression pattern in CFTR immunoprecipitates from CFBE410⁻ cells after 24 hr treatment with inh-2 (5 μ M), inh-5 (5 μ M), and VX-809 (1 μ M) in the absence or in the presence of MG-132 (10 μ M; last 4 hr) to block proteasomal degradation. (B–D) Analysis of intensity profiles of CFTR and ubiquitin in the absence (B) or in the presence of MG-132 (C and D).

(legend continued on next page)

ubiquitylation experiments to evaluate levels of ATG4B ubiquitylation in F508del-CFTR-expressing CFBE41o⁻ cells following 24 hr treatment with inh-2, inh-5 (both at 5 μ M), or, as negative control, vehicle alone (DMSO). In parallel, we also silenced cells with the anti-RNF5 siRNA molecule. After treatment, cells were lysed, and lysates were immunoprecipitated using an anti-ATG4B antibody. The immunoprecipitants were then subjected to SDS-PAGE followed by western blotting to evaluate the presence of ubiquitylated ATG4B (Figure 5A). The blotting detected two ATG4B bands, corresponding to differently ubiquitylated forms, at 52 and 57 KDa (presumably corresponding to mono- and biubiquitylated ATG4B), as already described by Kuang et al. (2012). As expected, ATG4B ubiquitylation is markedly reduced by RNF5 silencing compared with the control condition (Figure 5A). Similarly, incubation with inh-2 decreased the ATG4B ubiquitylation level, while inh-5 was not effective (Figure 5A). To further demonstrate the ability of the test compounds to inhibit ATG4B ubiquitylation, we performed *in vivo* ATG4B ubiquitylation experiments in F508del-CFTR-expressing CFBE41o⁻ cells following transient transfection of a plasmid coding for a ubiquitin with a triple-hemagglutinin tag (Ub-3xHA). The day after transfection, cells were treated with inh-2 and, in parallel, with analog-1 (Figure 5B). Ubiquitin overexpression did not alter ATG4B expression level. ATG4B was detected as a marked band at 52 KDa (corresponding to mono-ubiquitylated ATG4B) and a faint band at 46 KDa (corresponding to the non-ubiquitylated protein). However, ubiquitin overexpression significantly increased the polyubiquitylated forms, with bands at 76 and 85 KDa, as already reported by Kuang et al. (2012).

ATG4B is reported to regulate basal autophagy, while RNF5 knockdown increases basal autophagy by decreasing ATG4B ubiquitylation and thus its degradation (Kuang et al., 2012). We exploited known readouts of basal autophagy in F508del-CFTR-expressing CFBE41o⁻ cells transfected with NT- or RNF5-targeting siRNA (30 nM) or following 24 hr treatment with test compounds (5 μ M). Western blot tests were performed on whole cell lysates to quantify expression levels of LC3IIB and p62, two well-known autophagy markers (Klionsky et al., 2016). Treatment with torin-1 (20 nM), a known autophagy inducer, markedly increased the LC3IIB band's intensity (Figure 6A). Incubation with inh-2 alone, or downregulation of RNF5 in the absence or in the presence of inh-2, significantly increased to the same extent the intensity of the LC3IIB band, while analog-1 did not change band intensity (Figure 6A). In agreement with these results, SAR-405 (2 μ M), a potent inhibitor of the autophagic pathway, significantly increased expression of p62 (which accumulates when the autophagic process is inhibited), while torin-1 had no effect (Figure 6B). Incubation with analog-1 significantly increased the p62 band's intensity, while treatment with inh-2 or RNF5 downregulation were not effective (Figure 6B).

We then decided to evaluate the effect of inh-2 and its analog on the formation of autophagic vacuoles. Monodansylcadaverine (MDC) is a specific marker for autolysosomes (Biederbick et al., 1995). Indeed, MDC accumulates inside autophagosomes. After

fusion of autophagosomes with lysosomes, MDC fluorescence increases due to the acidic environment. Therefore, F508del-CFTR-expressing CFBE41o⁻ cells were transfected with a scrambled siRNA or an siRNA molecule targeting RNF5, and then treated for 24 hr with torin-1 (20 nM), SAR-405 (2 μ M), test compounds (5 μ M), VX-809 (1 μ M), or DMSO alone (vehicle). The cells were then loaded with MDC and evaluated by high-content confocal imaging to detect signal spots (corresponding to autophagic vacuoles) in each cell (Figure 6C). Determination of signal spots clearly demonstrated that the number of autophagic vacuoles was significantly increased following RNF5 silencing, or after treatment with torin-1 or inh-2. Combination of RNF5 silencing plus inh-2 or VX-809 plus inh-2 resulted in an increased number of spots, similar to the one observed upon incubation with inh-2 alone. In contrast, incubation with SAR-405 significantly decreased the number of autophagic vacuoles (Figure 6C). Restoring the basal autophagy has been proposed as a rescue strategy for the F508del-CFTR mutant (Tosco et al., 2016). We therefore sought to understand whether the F508del-CFTR rescue was caused by the increase in basal autophagy, which we observed following genetic suppression or pharmacological inhibition of RNF5. We reasoned that an autophagy inhibitor would block the rescue of mutant CFTR by RNF5 suppression. Thus, F508del-CFTR-expressing CFBE41o⁻ cells were transfected with an NT or RNF5-targeting siRNAs. The cells were then treated for 24 hr with DMSO alone or with SAR-405 (2 μ M) to inhibit autophagy. In a parallel experiment, F508del-CFTR-expressing CFBE41o⁻ cells were treated for 24 hr with inh-2 (5 μ M) or VX-809 (1 μ M) or DMSO alone (vehicle), in the absence or presence of SAR-405 (2 μ M). We then evaluated mutant CFTR activity with the YFP-based assay (Figure 6E). Interestingly, co-treatment with SAR-405 did not antagonize F508del-CFTR rescue following RNF5 silencing or inhibition. This demonstrates that the modulation of the autophagic pathway is a secondary effect of RNF5 suppression, but not the mechanism by which CFTR rescue is achieved (Figure 6E).

We then focused on paxillin, another known RNF5 target (Didier et al., 2003). Paxillin is a multidomain protein that localizes primarily to sites of cell adhesions, known as focal adhesions, which link the extracellular matrix to the actin cytoskeleton. RNF5 regulates paxillin ubiquitylation and localization, and therefore affects the actin cytoskeleton (Didier et al., 2003). Therefore, we performed a texture analysis of the actin cytoskeleton following treatment of CFBE41o⁻ F508del-CFTR cells upon different experimental conditions. After 24 hr incubation with test compounds (5 μ M) or vehicle (DMSO), cells were fixed, and the actin cytoskeleton was labeled using phalloidin conjugated to Alexa Fluor 647 fluorophore (Figure 7A). As calculated by Haralick's formula, actin signal contrast (calculated on 4 adjacent px) was significantly altered by treatment with compounds. In particular, inh-2 decreased the signal contrast (4 px), while analog-1 increased it (Figure 7B).

RNF5 is also reported to affect cell motility by regulating paxillin. In particular, RNF5 knockdown increases cell motility

(E) Immunoblot detection of mutant CFTR in whole lysates derived from CFBE41o⁻ cells treated with inh-2 (5 μ M), VX-809 (1 μ M), or inh-2 plus VX-809, at different time points following CHX-induced block of protein synthesis.

(F) Quantification of mutant CFTR (band B and band C) half-life in experiments detailed in (E). Data are expressed as means \pm SEM, n = 3.

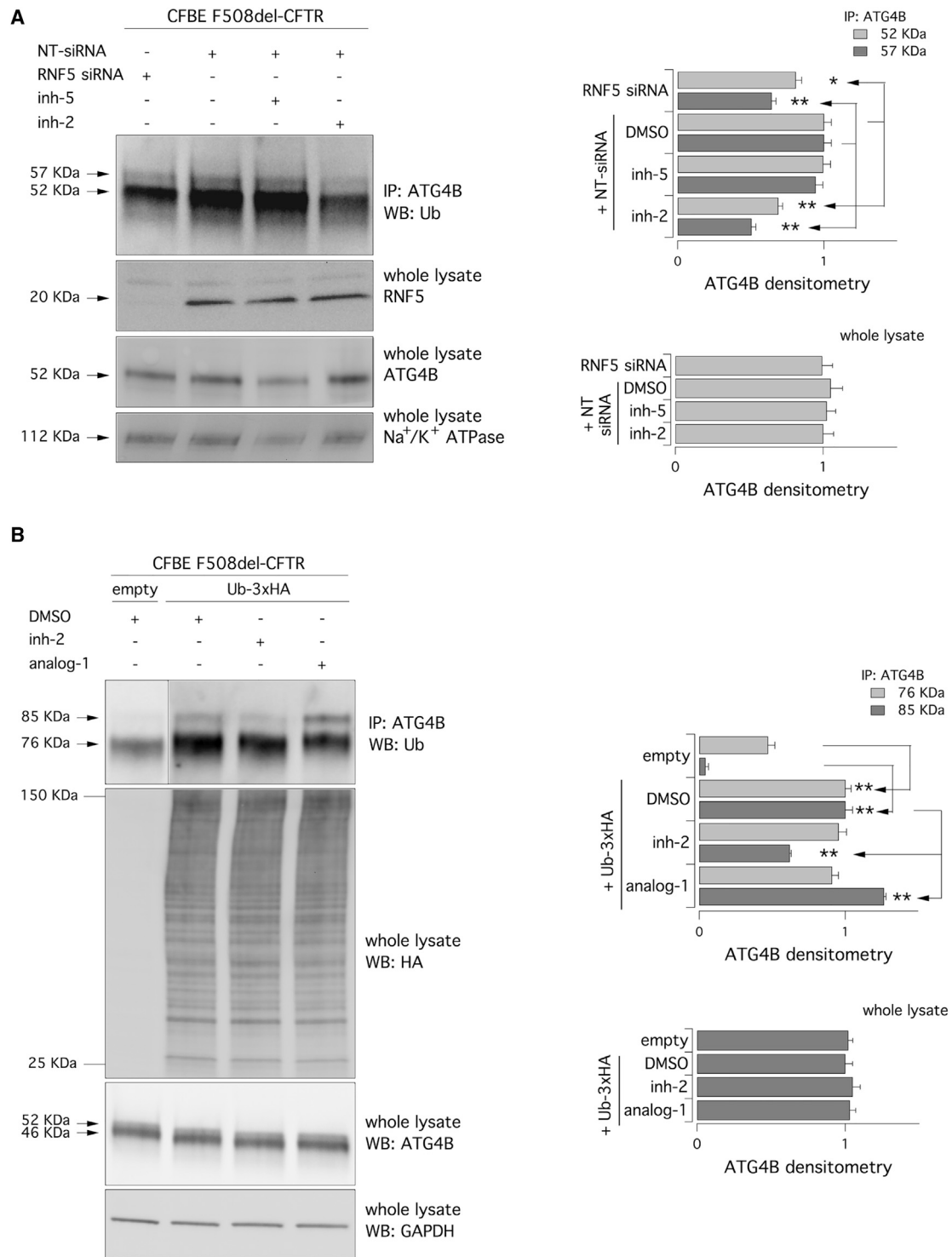


Figure 5. Evaluation of the Activity of Putative Hits as RNF5 Inhibitors: Effect on Downstream Target ATG4B

(A) Biochemical analysis of the ubiquitylation status of ATG4B in CFBE410⁻ cells treated with the indicated compounds (5 μ M), or following RNF5 silencing. (B) Biochemical analysis of the ubiquitylation status of ATG4B, following overexpression of ubiquitin (Ub-3xHA) in F508del-expressing CFBE410⁻ cells were transiently transfected with a tagged ubiquitin (Ub-3xHA) and treated with the indicated compounds (5 μ M). Data are expressed as means \pm SEM, n = 3. Symbols indicate statistical significance versus control: *p < 0.05, **p < 0.01.

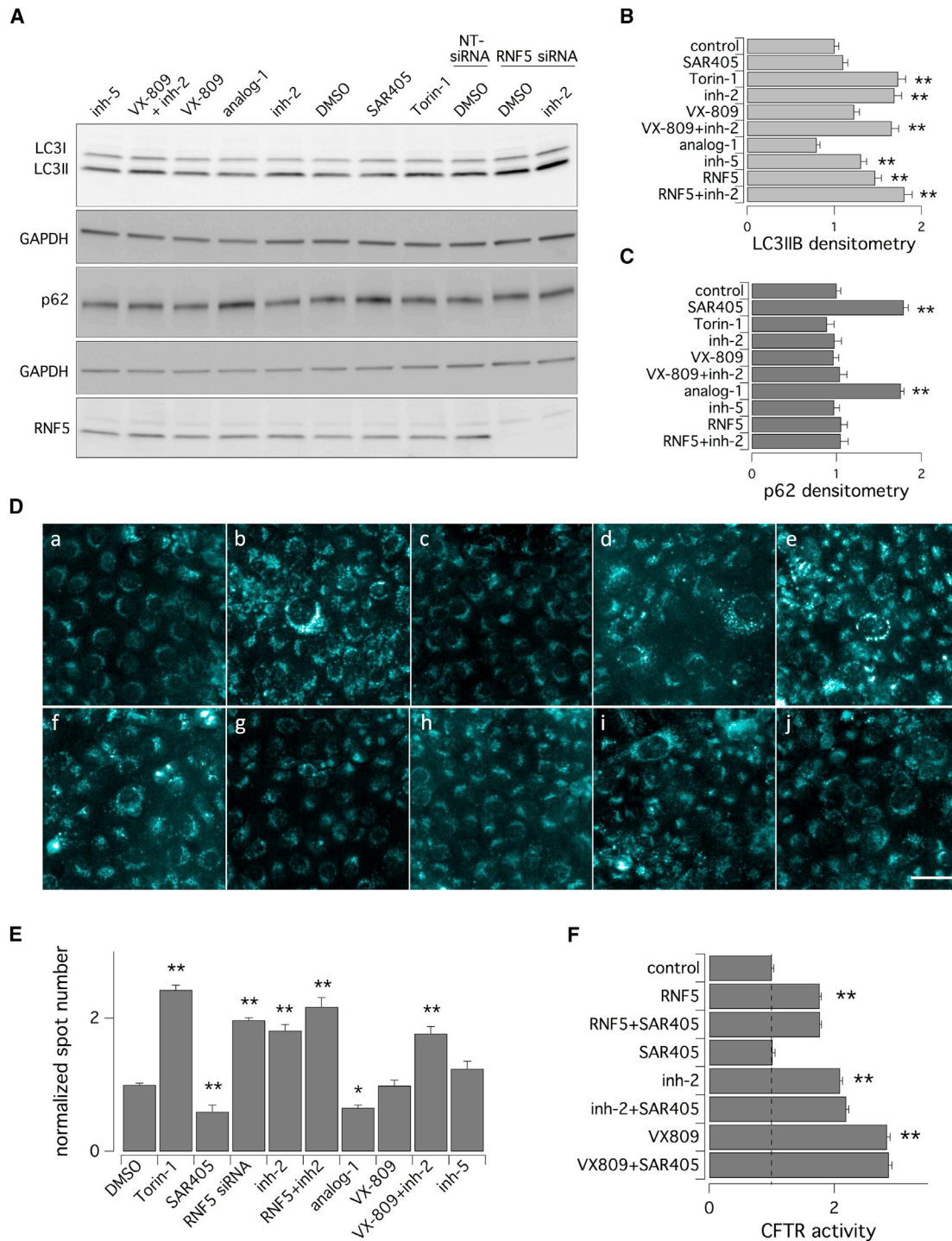


Figure 6. Evaluation of the Activity of Putative Hits as RNF5 Inhibitors: Effect on ATG4B-Mediated Basal Autophagy

(A) Biochemical analysis of LC3IIB and p62 in CFBE41o⁻ cells reversed transfected with NT- or RNF5-targeting siRNA or treated for 24 hr with DMSO, inh-2 (5 μM; e), analog-1 (5 μM; g), VX-809 (1 μM; h), VX-809 plus inh-2 (i), and inh-5 (5 μM), or treated for 3 hr with torin-1 (20 nM), or SAR-405 (2 μM).

(B and C) Quantification of LC3IIB and p62 expression in F508del-expressing CFBE41o⁻ cells treated as indicated in (A) Expression was normalized for the control condition (NT-siRNA or DMSO).

(D) Autophagic vacuoles in F508del-expressing CFBE41o⁻ cells transfected with NT-siRNA (or RNF5 siRNA) and treated with DMSO (a), torin-1 (20 nM; b), SAR-405 (2 μM; c), DMSO + anti-RNF5 siRNA (d), inh-2 (5 μM; e), anti-RNF5 siRNA plus inh-2 (f), analog-1 (5 μM; g), VX-809 (1 μM; h), VX-809 plus inh-2 (i), and inh-5 (5 μM; j), visualized after loading with MDC (50 μM). Scale bar, 100 μm.

(legend continued on next page)

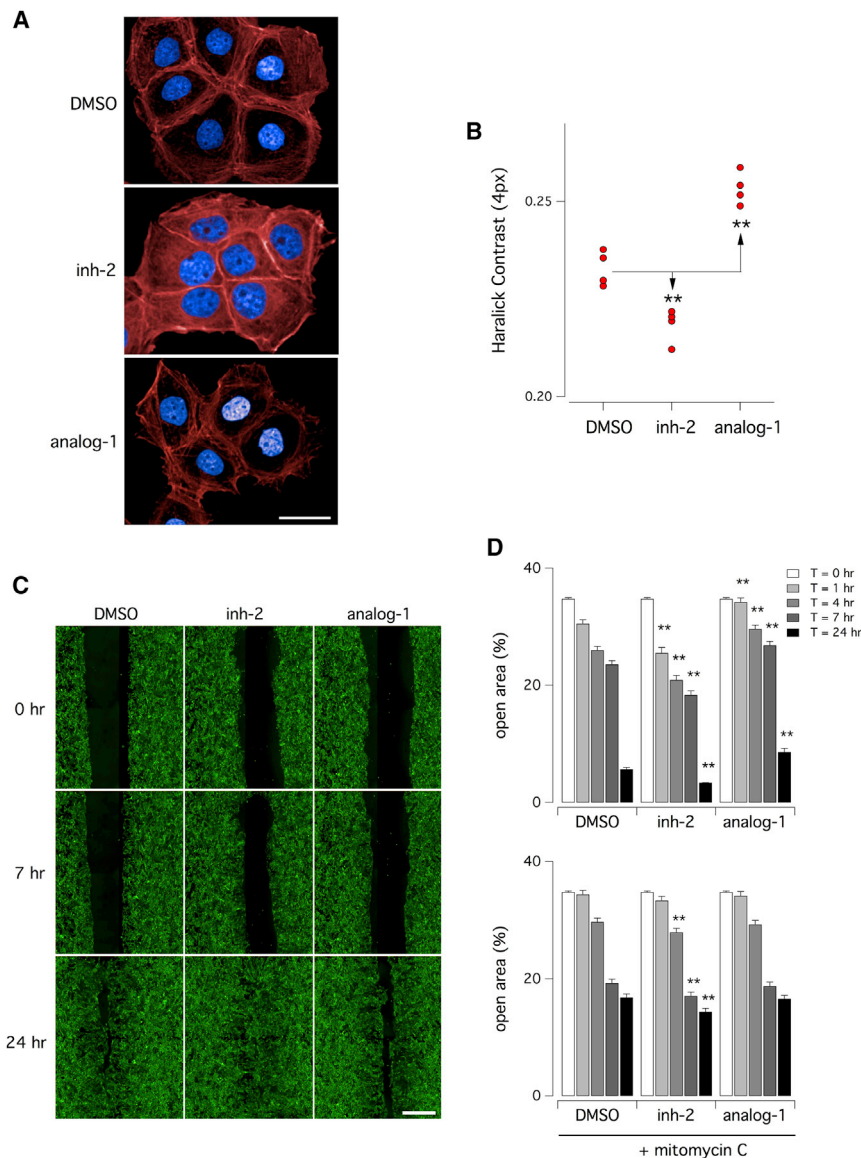


Figure 7. Evaluation of the Activity of Putative Hits as RNF5 Inhibitors: Effect on Downstream Target Paxillin

(A and B) Representative images and bar graph showing results of texture analysis of actin cytoskeleton labeled with phalloidin conjugated to Alexa Fluor 647, in F508del-CFTR-expressing CFBE410⁻ cells treated with the indicated compounds (5 μ M). Scale bar, 50 μ m.

(C and D) Representative images and bar graphs showing results of scratch wound healing assay performed on CFPAC-1 cells following 24 hr treatment with the indicated compounds (5 μ M), in the absence (upper panel) or presence (lower panel) of mitomycin C (30 μ M). Scale bar, 250 μ m. Data are expressed as means \pm SEM. Symbols indicate statistical significance versus respective control condition: ** p < 0.01.

to allow or block, respectively, cell proliferation. In both conditions, gap filling was significantly improved by treatment with inh-2 (Figures 7C and 7D).

DISCUSSION

A critical goal in CF research is the pharmacological rescue of processing and trafficking defects caused by the CFTR F508del mutation. This outcome may be achieved using pharmacological chaperones that directly interact with mutant CFTR to improve its folding and enhance its stability, or by blocking the activity of proteins that perturb CFTR trafficking and promote its premature degradation. Indeed, several proteins have been identified as potentially useful drug targets for a CF therapy based on proteostasis modulation (Balch et al., 2008; Amaral and Farinha, 2013; Sondo et al., 2017). Previously, our group compared the therapeutic

relevance of modulating these proteins using gene-silencing approaches, highlighting RNF5 as an interesting putative drug target (Tomati et al., 2015). RNF5 is an E3 ubiquitin ligase that acts at early stages of F508del-CFTR biosynthesis (Grove et al., 2009). RNF5 knockdown is particularly effective in rescuing mutant CFTR at the functional level in immortalized bronchial epithelial cells (Tomati et al., 2015). Our observations were validated using genetic animal models of RNF5KO (Delau-nay et al., 2008) and CFTR Δ F508 (van Doorninck et al., 1995; Bij-velds et al., 2005). Homozygous F508del-CFTR (CFTR Δ F508) mice show consistent intestinal malabsorption (Bijvelds et al.,

by decreasing paxillin ubiquitylation and thus its degradation (Didier et al., 2003). Therefore, we performed a scratch wound healing assay to evaluate whether incubation with inh-2 and its analog altered cell migration/proliferation (Figures 7C and 7D). We used CFPAC-1 cells because they are more firmly attached to the substrate compared with CFBE410⁻ cells. Moreover, they do not detach as a single cell sheet when injured. CFPAC-1 cells were plated on 96-well plates. After 24 hr, cell layers were scratched, and cells were treated with test compounds (5 μ M) or DMSO (vehicle). Experiments were performed in the absence or presence of mitomycin C

(E) Quantification of the number of autophagic vesicles (signal spots) in cells treated as indicated in (D), normalized for the control condition (cells transfected with the NT-siRNA and treated with DMSO).

(F) F508del-CFTR activity measured on CFBE410⁻ cells, using the YFP assay upon transfection with NT-siRNA (or RNF5 siRNA) and 24 hr treatment with indicated compounds (2 μ M SAR-405; 5 μ M inh-2; 1 μ M VX-809). Activity was normalized for the activity detected under control condition (cells transfected with the NT-siRNA and treated with DMSO). Data are expressed as means \pm SEM. Symbols indicate statistical significance versus control condition: * p < 0.05, ** p < 0.01.

2005; Freudenberg et al., 2008; Wilke et al., 2011), reduced intestinal cAMP-induced chloride and bicarbonate transport response (Wilke et al., 2011; Xiao et al., 2012), and a higher secretion of fecal biliary acids (Bijvelds et al., 2005; Freudenberg et al., 2008; Wilke et al., 2011). *In vivo* RNF5 suppression ameliorated these defects in CFTR Δ F508 mice (Tomati et al., 2015), providing a strong basis for developing molecules to inhibit RNF5 activity.

Here, we used computational methods to generate a homology model of RNF5 RING domain (starting from the structures of the RING domains of other proteins) to perform virtual screening based on ligand docking. In parallel, we used molecular fingerprinting to select a diversity set of compounds.

To increase the chances of successfully identifying RNF5 inhibitors, we adopted two complementary computational approaches. Careful computational modeling was required for the very low sequence identity with the templates available for the homology modeling, and for the very high flexibility of protein. In particular, we used ten different protein conformations in the virtual screening protocol to deal with the high protein flexibility. Using these conformations, a first set of 1,623 ligands was selected by high-throughput docking. A second diversity set of 1,000 ligands based on molecular fingerprint chemical diversity was extracted.

We used the functional assay based on HS-YFP to evaluate the biological activity of selected compounds as F508del-CFTR correctors. Our group has used this assay extensively to identify and characterize CFTR correctors (Pedemonte et al., 2005, 2010, 2011). In total, 43 hits were identified in the primary screening on CFBE41o⁻ cells. The hit rate of 1.5% was very high compared with that obtained in previous screenings (Pedemonte et al., 2005, 2010), suggesting that the compound set was enriched by molecules acting as F508del-correctors. Surprisingly, we observed an extremely low hit-confirmation rate, with only two compounds having a clear dose-dependent effect. The remaining 41 compounds, however, should not be considered false positives. Their corrector activity was consistently detected but only at one or two of the concentrations tested, with toxic effects at higher concentrations. These disappointing results could be explained by their putative mechanism of action, involving inhibition of ubiquitin ligases. Indeed, while RNF5 suppression has no apparent negative effect *in vitro* or *in vivo*, as shown in this and in previous reports (Delaunay et al., 2008; Tomati et al., 2015), primary hits could also inhibit activity of ligases other than RNF5, leading to toxic side effects.

We used two different electrophysiological techniques to evaluate the best hits as F508del-CFTR correctors on human primary bronchial epithelia. The compound named inh-2 rescued the F508del-CFTR processing defect, increasing CFTR-mediated current. Surprisingly, a close analog of inh-2 (analog-1), as well as inh-5, had no activity as correctors. Co-treatment with inh-2 and analog-1 resulted in a complete loss of F508del-CFTR rescue by inh-2. In the case of inh-5, we can speculate that lack of consistency between results obtained in immortalized and primary bronchial cells could be due to possible effects on other targets that, in primary cells, hinder mutant CFTR rescue.

Evaluation of the mechanism of action of inh-2, leading to CFTR rescue, confirmed that this compound decreases ubiquitylation of mutant CFTR, thus stabilizing the mature form of CFTR (but not the immature one, band B). This is in contrast with what has been described, for example, for FAU suppression (another possible target involved in F508del-CFTR maturation) that extends the half-life of both mature and immature CFTR (Tomati et al., 2018).

To further investigate the mechanism of action of inh-2 (and its analog), we exploited known cellular targets of RNF5, other than CFTR. First, we examined the ubiquitylation level of ATG4B, which is mediated by RNF5 (Kuang et al., 2012). *In vivo* ubiquitylation experiments confirmed that inh-2 inhibits RNF5 ligase activity, decreasing the ubiquitylated forms of ATG4B. Interestingly, treatment with analog-1 increased the ubiquitylation status of ATG4B. Treatment with inh-5 did not affect ATG4B ubiquitylation. We can speculate that inh-5 inhibits a ubiquitin ligase involved in CFTR ubiquitylation (in immortalized but not in primary bronchial cells), different from RNF5.

ATG4B is reported to be a regulator of basal autophagy (Kuang et al., 2012). Treatment of cells with inh-2 increased the basal level of autophagy, as demonstrated by functional (increased MDC signal spots) and biochemical evidence (increased intensity of LC3IIB band and decreased intensity of p62 band). These results are in agreement with the finding that cysteine protease ATG4B is responsible for regulating LC3 processing (Kuang et al., 2012). Treatment with analog-1 caused the opposite effects (compared to inh-2). Restoring the basal autophagy has been proposed as a rescue strategy for the F508del-CFTR mutant (Tosco et al., 2016). Here, however, the increase in basal autophagy appeared to be a secondary effect of RNF5 inhibition, rather than the cause of mutant CFTR rescue.

We also evaluated the effect of inh-2 and analog-1 on another RNF5 target, paxillin (Didier et al., 2003). Paxillin localizes in focal adhesions, which link extracellular matrix to the actin cytoskeleton (Turner, 2000). By increasing paxillin ubiquitylation, RNF5 overexpression alters the actin cytoskeleton and decreases cell motility (Didier et al., 2003). Thus, we analyzed the texture pattern of the actin cytoskeleton, which was consistently altered by treatment with both inh-2 and analog-1, although with opposite effects. Scratch/wound healing assays confirmed that inh-2 increases cell motility, improving gap filling in the cell layer, which is consistent with inhibition of RNF5 ubiquitin ligase activity. In contrast, treatment with analog-1 significantly delayed gap filling.

In summary, our findings demonstrate that inh-2 acts as an RNF5 inhibitor, modulating RNF5 downstream targets. We cannot exclude that inh-2 could also affect other targets; however, the biological effects that we observed after treatment with inh-2 are consistent with what has been described as RNF5-dependent. Thus, inh-2 could inhibit for example other ubiquitin ligases involved in the same pathways of RNF5. We hypothesize that inh-2 directly binds to RNF5 RING domain thus inhibiting RNF5 ligase activity. The proposed binding mode (Figure S1) based on docking simulations of inh-2 into the homology model of RNF5 shows an H-bond between our compound and Arg73, two π - π interactions with Trp48 and

His52, and some hydrophobic interactions with Leu55, Val38, and Val76. Despite this binding mode should be considered rather preliminary, it can offer the possibility to rationally modify and optimize inh-2 through a medicinal chemistry campaign, which can in turn help in better understanding the binding mode and optimizing the homology model.

Experimental evidence suggests also that analog-1 could be an RNF5 activator, eliciting the opposite effects on RNF5 targets downstream as compared with inh-2. Indeed, the ability of inh-2 to rescue the F508del-CFTR trafficking defect is completely reversed by co-treatment with analog-1. Notably, although pharmacological modulation of RNF5 has a significant impact on cell motility, basal autophagy, and possibly other cell processes, mice lacking RNF5 expression display no altered phenotypes (Delaunay et al., 2008). This suggests that *in vivo* RNF5 inhibition could be exploited. In addition, RNF5 knockout mice have been shown to be resistant to group A streptococcus infection, in part due to enhanced autophagy-mediated clearance of invading bacteria by macrophages (Kuang et al., 2012). Indeed, *in vivo* RNF5 regulation of autophagy is involved in the innate host defense against bacterial infection. This could be considered a positive secondary effect of RNF5 inhibition in CF patients having chronic lung infection. However, it has also been demonstrated that RNF5 negatively regulates virus-triggered induction of type I IFNs and cellular antiviral response by targeting both VISA and MITA (Zhong et al., 2010). Thus, *in vivo* RNF5 inhibition could lead to deregulated cellular antiviral response.

Taken together, our findings demonstrate that RNF5 inhibition can rescue the F508del-CFTR trafficking defect, not only in heterologous cell lines or in a murine CF model, but also in primary culture of human bronchial epithelia, the main target tissue for CF treatment. These findings validate RNF5 as a drug target for CF, and provide evidence to support its druggability.

SIGNIFICANCE

In cystic fibrosis (CF), deletion of phenylalanine 508 (F508del) in the CFTR channel is associated with misfolding and premature degradation of the mutant protein. Correctors are molecules that improve the maturation and trafficking of F508del-CFTR to the membrane. Correctors could act by improving CFTR folding and processing or as proteostasis regulators, i.e., modulating the proteostasis environment thus leading to beneficial effects on CFTR processing. Among the known proteins associated with F508del-CFTR processing, the ubiquitin ligase RNF5/RMA1 is particularly interesting. Genetic suppression of RNF5 *in vivo* leads to an attenuation of intestinal pathological phenotypes in CF mice, validating the therapeutic relevance of this target for CF pathology. Here, we used a computational approach to discover inh-02, a drug-like small molecule that inhibits RNF5. Inh-2 rescues F508del-CFTR processing defect in primary bronchial epithelia from CF patients. Analysis of inh-2 mechanism of action confirmed that it decreases CFTR ubiquitylation, thus increasing its half-life. This work validates RNF5 as a drug target for CF, providing evidence to support its druggability.

STAR★METHODS

Detailed methods are provided in the online version of this paper and include the following:

- KEY RESOURCES TABLE
- CONTACT FOR REAGENTS AND RESOURCE SHARING
- EXPERIMENTAL MODEL AND SUBJECT DETAILS
- METHOD DETAILS
 - Homology Modeling
 - Molecular Dynamics
 - Life Chemicals Database Preparation
 - Virtual Screening by High-Throughput Docking
 - Diversity Set Selection
 - Compound Library Screening
 - Synthesis of Compounds
 - Synthetic Procedures to Obtain Compounds inh-2, analog-1, and Intermediates 1-2
 - Purification of inh-2 and analog-1
 - NMR Purity Assessment and Structural Elucidation of inh-2 and analog-1
 - Final Purity and Chemical Structures Data for inh-2 and analog-1
 - Gene Silencing by siRNA Transfection
 - Fluorescence Assay for CFTR
 - Transepithelial Electrical Resistance and Potential Difference Measurements (TEER/PD)
 - Short-Circuit Current Recordings
 - CFTR Immunoprecipitation (IP) Assay
 - Western Blot
 - Proliferation Study
 - MTT Tetrazolium Cell Viability Assay
 - In Vivo Ubiquitylation Assay
 - Labeling of Autophagic Vacuoles with Monodansylcaverine (MDC)
 - Analysis of Actin Cytoskeleton
 - Scratch Wound Healing Assay
- QUANTIFICATION AND STATISTICAL ANALYSIS

SUPPLEMENTAL INFORMATION

Supplemental Information includes one figure and one table and can be found with this article online at <https://doi.org/10.1016/j.chembiol.2018.04.010>.

ACKNOWLEDGMENTS

The authors thank Dr. Aldamaria Puliti, Dr. Renata Bocciardi, and Dr. Luis J. V. Galletta for critical readings of the manuscript and helpful suggestions. The authors thank Mr. Giuseppe Nicora and Mr. Carlo Pedemonte for their valuable assistance with the Ussing chamber equipment. This work was supported by Ricerca Corrente from the Italian Ministry of Health (Linea1), by ERA-Net for Research Programmes on Rare Diseases (E-RARE 3; "INSTINCT"), by grants from the Fondazione per la Ricerca sulla Fibrosi Cistica to A.C. (FFC no. 2/2015 with the contribution of "Delegazioni FFC di Verona e di Tradate Gallarate," "La Notte dei Saporì"; and "Audemars Piguet Italia") and to N.P. (FFC no. 5/2012 with the contribution of "Danone S.p.A."; FFC no. 9/2017 with the contribution of "Delegazione FFC di Genova e Gruppo di Sostegno FFC di Savona Spotorno," "Un fiore per Valeria [Assemini - Cagliari]," "Gruppo di Sostegno FFC di Vigevano," "Delegazione FFC della Valdadige," and "Delegazione FFC di Lodi").

AUTHOR CONTRIBUTIONS

E.S. performed the biological evaluation of selected compounds, with the help of V.T. F.F. generated the homology model of RNF5 RING domain and performed the virtual screening. E.G. synthesized the test compounds, which were purified and quality-checked by S.M.B., L.G., and A.A. E.P. performed the cadaverine assay. Primary bronchial epithelial cells were cultured by E.C., who also performed the short-circuit current measurements. L.F. performed transepithelial electrical resistance measurements on cell lines and primary bronchial epithelia. A.C. supervised the computational studies. N.P. analyzed biological data. R.R., N.P., and A.C. planned the study. N.P. wrote the manuscript, aided by F.F., E.S., R.R., and A.C.

DECLARATION OF INTERESTS

The authors have declared that no conflict of interest exists.

Received: November 14, 2017

Revised: February 22, 2018

Accepted: April 9, 2018

Published: May 10, 2018

REFERENCES

- Amaral, M.D., and Farinha, C.M. (2013). Rescuing mutant CFTR: a multi-task approach to a better outcome in treating cystic fibrosis. *Curr. Pharm. Des.* *19*, 3497–3508.
- Balch, W.E., Morimoto, R.I., Dillin, A., and Kelly, J.W. (2008). Adapting proteostasis for disease intervention. *Science* *319*, 916–919.
- Biederbick, A., Kern, H.F., and Elsässer, H.P. (1995). Monodansylcadaverine (MDC) is a specific in vivo marker for autophagic vacuoles. *Eur. J. Cell Biol.* *66*, 3–14.
- Bijvelds, M.J.C., Bronsveld, I., Havinga, R., Sinaasappel, M., de Jonge, H.R., and Verkade, H.J. (2005). Fat absorption in cystic fibrosis mice is impeded by defective lipolysis and post-lipolytic events. *Am. J. Physiol. Gastrointest. Liver Physiol.* *288*, 646–653.
- Dalemans, W., Barbry, P., Champigny, G., Jallat, S., Dott, K., Dreyer, D., Crystal, R.G., Pavirani, A., Lecocq, J.P., and Lazdunski, M. (1991). Altered chloride ion channel kinetics associated with the delta F508 cystic fibrosis mutation. *Nature* *354*, 526–528.
- Delaunay, A., Bromberg, K.D., Hayashi, Y., Mirabella, M., Burch, D., Kirkwood, B., Serra, C., Malicdan, M.C., Mizisin, A.P., Morosetti, R., et al. (2008). The ER-bound RING finger protein 5 (RNF5/RMA1) causes degenerative myopathy in transgenic mice and is deregulated in inclusion body myositis. *PLoS One* *3*, e1609.
- Didier, C., Broday, L., Bhoumik, A., Israeli, S., Takahashi, S., Nakayama, K., Thomas, S.M., Turner, C.E., Henderson, S., Sabe, H., and Ronai, Z. (2003). RNF5, a RING finger protein that regulates cell motility by targeting paxillin ubiquitination and altered localization. *Mol. Cell Biol.* *23*, 5331–5345.
- Du, K., Sharma, M., and Lukacs, G.L. (2005). The DeltaF508 cystic fibrosis mutation impairs domain-domain interactions and arrests post-translational folding of CFTR. *Nat. Struct. Mol. Biol.* *12*, 17–25.
- Freudenberg, F., Broderick, A.L., Yu, B.B., Leonard, M.R., Glickman, J.N., and Carey, M.C. (2008). Pathophysiological basis of liver disease in cystic fibrosis employing a DeltaF508 mouse model. *Am. J. Physiol. Gastrointest. Liver Physiol.* *294*, 1411–1420.
- Grove, D.E., Rosser, M.F.N., Ren, H.Y., Naren, A.P., and Cyr, D.M. (2009). Mechanisms for rescue of correctable folding defects in CFTRDelta F508. *Mol. Biol. Cell* *20*, 4059–4069.
- Haralick, R.M., Shanmugam, K., and Dinstein, I. (1973). Textural features for image classification. *IEEE Trans. Syst. Man Cybern.* *3*, 610–621.
- Klionsky, D.J., Abdelmohsen, K., Abe, A., Abedin, M.J., Abeliovich, H., Acevedo Arozena, A., Adachi, H., Adams, C.M., Adams, P.D., Adeli, K., et al. (2016). Guidelines for the use and interpretation of assays for monitoring autophagy (3rd edition). *Autophagy* *12*, 1–222.
- Kuang, E., Okumura, C.Y., Sheffy-Levin, S., Varsano, T., Shu, V.C., Qi, J., Niesman, I.R., Yang, H.J., López-Otín, C., Yang, W.Y., et al. (2012). Regulation of ATG4B stability by RNF5 limits basal levels of autophagy and influences susceptibility to bacterial infection. *PLoS Genet.* *8*, e1003007.
- Ma, T., Thiagarajah, J.R., Yang, H., Sonawane, N.D., Folli, C., Galiotta, L.J., and Verkman, A.S. (2002). Thiazolidinone CFTR inhibitor identified by high-throughput screening blocks cholera toxin-induced intestinal fluid secretion. *J. Clin. Invest.* *110*, 1651–1658.
- Okiyonedo, T., Veit, G., Dekkers, J.F., Bagdany, M., Soya, N., Xu, H., Roldan, A., Verkman, A.S., Kurth, M., Simon, A., et al. (2013). Mechanism-based corrector combination restores Δ F508-CFTR folding and function. *Nat. Chem. Biol.* *9*, 444–454.
- Pedemonte, N., Tomati, V., Sondo, E., Caci, E., Millo, E., Armirotti, A., Damonte, G., Zegarra-Moran, O., and Galiotta, L.J. (2011). Dual activity of aminoarylthiazoles on the trafficking and gating defects of the cystic fibrosis transmembrane conductance regulator chloride channel caused by cystic fibrosis mutations. *J. Biol. Chem.* *286*, 15215–15226.
- Pedemonte, N., Lukacs, G.L., Du, K., Caci, E., Zegarra-Moran, O., Galiotta, L.J., and Verkman, A.S. (2005). Small-molecule correctors of defective DeltaF508-CFTR cellular processing identified by high-throughput screening. *J. Clin. Invest.* *115*, 2564–2571.
- Pedemonte, N., Tomati, V., Sondo, E., and Galiotta, L.J.V. (2010). Influence of cell background on pharmacological rescue of mutant CFTR. *Am. J. Physiol. Cell Physiol.* *298*, C866–C874.
- Pesce, E., Bellotti, M., Liessi, N., Guariento, S., Damonte, G., Cichero, E., Galatini, A., Salis, A., Gianotti, A., Pedemonte, N., et al. (2015). Synthesis and structure-activity relationship of aminoarylthiazole derivatives as correctors of the chloride transport defect in cystic fibrosis. *Eur. J. Med. Chem.* *99*, 14–35.
- Pesce, E., Gorrieri, G., Sirci, F., Napolitano, F., Carrella, D., Caci, E., Tomati, V., Zegarra-Moran, O., di Bernardo, D., and Galiotta, L.J. (2016). Evaluation of a systems biology approach to identify pharmacological correctors of the mutant CFTR chloride channel. *J. Cyst. Fibros.* *15*, 425–435.
- Pilewski, J.M., and Frizzell, R.A. (1999). Role of CFTR in airway disease. *Physiol. Rev.* *79*, S215–S255.
- Reynès, C., Host, H., Camproux, A.C., Laconde, G., Leroux, F., Mazars, A., Deprez, B., Fahraeus, R., Villoutreix, B.O., and Sperandio, O. (2010). Designing focused chemical libraries enriched in protein-protein interaction inhibitors using machine-learning methods. *PLoS Comput. Biol.* *6*, e1000695.
- Scudieri, P., Caci, E., Bruno, S., Ferrera, L., Schiavon, M., Sondo, E., Tomati, V., Gianotti, A., Zegarra-Moran, O., Pedemonte, N., et al. (2012). Association of TMEM16A chloride channel overexpression with airway goblet cell metaplasia. *J. Physiol.* *590*, 6141–6155.
- Sondo, E., Tomati, V., Caci, E., Esposito, A.I., Pfeffer, U., Pedemonte, N., and Galiotta, L.J. (2011). Rescue of the mutant CFTR chloride channel by pharmacological correctors and low temperature analyzed by gene expression profiling. *Am. J. Physiol. Cell Physiol.* *301*, C872–C885.
- Sondo, E., Pesce, E., Tomati, V., Marini, M., and Pedemonte, N. (2017). RNF5, DAB2 and friends: novel drug targets for cystic fibrosis. *Curr. Pharm. Des.* *23*, 176–186.
- The UniProt Consortium. (2017). UniProt: the universal protein knowledge-base. *Nucleic Acids Res.* *46*, 2699.
- Tomati, V., Sondo, E., Armirotti, A., Caci, E., Pesce, E., Marini, M., Gianotti, A., Jeon, Y.J., Cilli, M., Pistorio, A., et al. (2015). Genetic inhibition of the ubiquitin ligase RNF5 attenuates phenotypes associated to F508del cystic fibrosis mutation. *Sci. Rep.* *5*, 12138.
- Tomati, V., Pesce, E., Caci, E., Sondo, E., Scudieri, P., Marini, M., Amato, F., Castaldo, G., Ravazzolo, R., Galiotta, L.J.V., and Pedemonte, N. (2018). High-throughput screening identifies FAU protein as a regulator of mutant cystic fibrosis transmembrane conductance regulator channel. *J. Biol. Chem.* *293*, 1203–1217.
- Tosco, A., De Gregorio, F., Esposito, S., De Stefano, D., Sana, I., Ferrari, E., Sepe, A., Salvadori, L., Buonpensiero, P., Di Pasqua, A., et al. (2016). A novel treatment of cystic fibrosis acting on-target: cysteamine plus epigallocatechin

- gallate for the autophagy-dependent rescue of class II-mutated CFTR. *Cell Death Differ.* **8**, 1380–1393.
- Tradtrantip, L., Sonawane, N.D., Namkung, W., and Verkman, A.S. (2009). Nanomolar potency pyrimido-pyrrolo-quinoxalinedione CFTR inhibitor reduces cyst size in a polycystic kidney disease model. *J. Med. Chem.* **52**, 6447–6455.
- Turner, M.R. (1986). Texture discrimination by Gabor functions. *Biol. Cybern.* **55**, 71–82.
- Turner, C.E. (2000). Paxillin and focal adhesion signalling. *Nat. Cell Biol.* **12**, E231–E236.
- van Doorninck, J.H., French, P.J., Verbeek, E., Peters, R.H., Morreau, H., Bijman, J., and Scholte, B.J. (1995). A mouse model for the cystic fibrosis delta F508 mutation. *EMBO J.* **14**, 4403–4411.
- Wainwright, C.E., Elborn, J.S., Ramsey, B.W., Marigowda, G., Huang, X., Cipolli, M., Colombo, C., Davies, J.C., De Boeck, K., Flume, P.A., et al.; TRAFFIC and TRANSPORT Study Groups (2015). Lumacaftor-ivacaftor in patients with cystic fibrosis homozygous for phe508del CFTR. *N. Engl. J. Med.* **373**, 220–231.
- Wider, G., and Dreier, L. (2006). Measuring protein concentrations by NMR spectroscopy. *J. Am. Chem. Soc.* **128**, 2571–2576.
- Wilke, M., Buijs-Offerman, R.M., Aarbiou, J., Colledge, W.H., Sheppard, D.N., Touqui, L., Bot, A., Jorna, H., de Jonge, H.R., and Scholte, B.J. (2011). Mouse models of cystic fibrosis: phenotypic analysis and research applications. *J. Cyst. Fibros.* **10**, S152–S171.
- Wu, P.S., and Otting, G. (2005). Rapid pulse length determination in high-resolution NMR. *J. Magn. Reson.* **176**, 115–119.
- Xiao, F., Li, J., Singh, A.K., Riederer, B., Wang, J., Sultan, A., Park, H., Lee, M.G., Lamprecht, G., Scholte, B.J., et al. (2012). Rescue of epithelial HCO₃-secretion in murine intestine by apical membrane expression of the cystic fibrosis transmembrane conductance regulator mutant F508del. *J. Physiol.* **590**, 5317–5334.
- Younger, J.M., Chen, L., Ren, H.Y., Rosser, M.F., Turnbull, E.L., Fan, C.Y., Patterson, C., and Cyr, D.M. (2006). Sequential quality-control checkpoints triage misfolded cystic fibrosis transmembrane conductance regulator. *Cell.* **126**, 571–582.
- Yu, H., Burton, B., Huang, C.J., Worley, J., Cao, D., Johnson, J.P., Jr., Urrutia, A., Joubran, J., Seepersaud, S., Sussky, K., et al. (2012). Ivacaftor potentiation of multiple CFTR channels with gating mutations. *J. Cyst. Fibros.* **11**, 237–245.
- Zhong, B., Zhang, Y., Tan, B., Liu, T.T., Wang, Y.Y., and Shu, H.B. (2010). The E3 ubiquitin ligase RNF5 targets virus-induced signaling adaptor for ubiquitination and degradation. *J. Immunol.* **184**, 6249–6255.

STAR★METHODS

KEY RESOURCES TABLE

REAGENT or RESOURCE	SOURCE	IDENTIFIER
Antibodies		
Rabbit monoclonal anti-ATG4B (D1G2R)	Cell Signaling Technology	Cat#13507
Rabbit polyclonal anti-LC3B	Sigma	Cat#L7543; RRID: AB_796155
Rabbit polyclonal anti-SQTM1/p62	Cell Signaling Technology	Cat#5114
Mouse monoclonal anti-RNF5 antibody (22B3)	Santa Cruz Biotechnology	Cat#sc-81716; RRID: AB_2238618
Mouse monoclonal anti-GAPDH (6C5)	Santa Cruz Biotechnology	Cat#sc-32233; RRID: AB_627679
Mouse monoclonal anti-Ub (P4D1)	Santa Cruz Biotechnology	Cat#sc-8017; RRID: AB_628423
Horseradish peroxidase (HRP)-conjugated mouse monoclonal anti-Ub (P4D1-HRP)	Santa Cruz Biotechnology	Cat#sc-8017-HRP
Mouse monoclonal anti-CFTR (596)	Cystic Fibrosis Foundation Therapeutics	ID: 596
Mouse monoclonal anti-CFTR (24-1)	R&D Systems	Cat#MAB25031; RRID: AB_2260673
Mouse monoclonal anti Na ⁺ /K ⁺ ATPase α 1 (C464.6)	Millipore	Cat#05-369; RRID: AB_309699
Monoclonal antibody anti- HA.11 (16B12)	Biologend	Cat#901514; RRID: AB_2565336
HRP-conjugated anti-mouse IgG	Abcam	Cat#ab6789; RRID: AB_955439
HRP-conjugated anti-rabbit IgG	DAKO	Cat#P0448; RRID: AB_2617138
HRP-conjugated anti-HA (16B12)	Biologend	Cat#901519; RRID: AB_2686981
Chemicals, Peptides, and Recombinant Proteins		
VX-809	Selleck Chemicals	Cat#S1565
VX-770	Selleck Chemicals	Cat#S1144
CFTR inhibitor 172	Selleck Chemicals	Cat#S7139
PPQ102	Calbiochem	Cat#219677
Forkolin	Sigma	Cat#F6886
Genistein	Sigma	Cat#G6649
Experimental Models: Cell Lines		
Rat: Fischer rat thyroid (FRT) cells	Gaslini cell bank	N/A
Human: CFBE41o ⁻ (unknown age and gender)	Laboratory of John P Clancy	N/A
Human: CFBE41o ⁻ wt-CFTR (unknown age and gender)	Laboratory of John P Clancy	N/A
Human: CFBE41o ⁻ F508del-CFTR (unknown age and gender)	Laboratory of John P Clancy	N/A
Human: Primary CF-HBE F508del/F508del (unknown age and gender)	Gaslini cell bank	Donor ID: BE86
Human: Primary CF-HBE F508del/F508del (unknown age and gender)	Gaslini cell bank	Donor ID: BE91
Human: Primary CF-HBE F508del/F508del (unknown age and gender)	Gaslini cell bank	Donor ID: BE93
Human: Primary CF-HBE F508del/F508del (unknown age and gender)	Gaslini cell bank	Donor ID: BE111
Human: CFPAC-1 (26 yrs; male)	ATCC	Cat#CRL-1918
Oligonucleotides		
Anti-RNF5 siRNA	Life Technologies	Cat#HSS184327
siRNA negative control	Life Technologies	ID: MED GC
Recombinant DNA		
Plasmid: Ub-3xHA	VectorBuilder	custom

(Continued on next page)

Continued

REAGENT or RESOURCE	SOURCE	IDENTIFIER
Software and Algorithms		
Protein Preparation Wizard	Schrödinger	https://www.schrodinger.com/protein-preparation-wizard
Desmond	Schrödinger	https://www.schrodinger.com/desmond
LigPrep	Schrödinger	https://www.schrodinger.com/LigPrep
PPI-HitProfiler tool	Reynès et al., 2010	http://www.cdithem.fr/online.php?lg=en&service=ppiHitProfiler
SiteMap	Schrödinger	https://www.schrodinger.com/sitemap
Glide	Schrödinger	https://www.schrodinger.com/glide
Canvas	Schrödinger	https://www.schrodinger.com/canvas

CONTACT FOR REAGENTS AND RESOURCE SHARING

Further information and requests for reagents may be directed to, and will be fulfilled by the lead contact and corresponding author for biological studies Nicoletta Pedemonte (nicoletta.pedemonte@unige.it) or by the corresponding author for computational studies Andrea Cavalli (andrea.cavalli@unibo.it).

EXPERIMENTAL MODEL AND SUBJECT DETAILS

We generated CFBE410⁻ and FRT cells stably expressing F508del-CFTR and the halide-sensitive yellow fluorescent protein (HS-YFP) YFP-H148Q/I152L, as previously described (Sondo et al., 2011). As culture media, we used MEM for CFBE410⁻ cells and F-12 Coon's modification for FRT cells, both supplemented with 10% fetal calf serum, 2 mM L-glutamine, 100 U/ml penicillin, and 100 µg/ml streptomycin. For YFP-based assays of CFTR activity, CFBE410⁻ or FRT cells were plated (50,000 cells/well) on clear-bottom 96-well black microplates (Corning Life Sciences, Acton, MA).

The isolation, culture, and differentiation methods of primary bronchial epithelial cells have previously been described in detail (Scudieri et al., 2012). In brief, epithelial cells were obtained from mainstem bronchi of CF individuals undergoing lung transplant. No information about gender and age of the transplanted patients was provided to cell final users. For this study, cells were obtained from four CF patients (homozygous for F508del mutation). Bronchi were set overnight at 4°C in a solution containing protease XIV to detach cells. Epithelial cells were then cultured in a serum-free medium (LHC9 mixed with RPMI 1640, 1:1) supplemented with hormones and supplements that favor cell-number amplification. For cells deriving from CF patients, the culture medium contained a complex mixture of antibiotics (usually colistin, piperacillin, and tazobactam) to eradicate bacteria in the first days. The Ethics Committee of the Istituto Giannina Gaslini specifically approved the collection of bronchial epithelial cells and their study to investigate the mechanisms of transepithelial ion transport, following the guidelines of the Italian Ministry of Health. Each patient provided informed consent to the study using a form that was also approved by the Ethics Committee.

To obtain differentiated epithelia, cells were seeded at high density on porous membranes (500.000 cells for 1 cm² Snapwell inserts, Corning, code 3801, for Ussing chamber studies, or 200.000 cells for 0.33 cm² mini-transwell inserts, Corning, code 3379, for TEER/PD measurements). After 24 hr, the serum-free medium was replaced with DMEM/Ham's F12 containing 2% fetal bovine serum plus hormones and supplements. Differentiation of cells into a tight epithelium was checked by measuring transepithelial electrical resistance and potential difference with an epithelial voltohmmeter (EVOM1, World Precision Instruments). The medium was replaced daily on both sides of permeable supports up to 8–10 days (liquid-liquid culture, LLC). Subsequently the apical medium was totally removed, and the cells received nutrients only from the basolateral side (air-liquid culture, ALC). This condition favored a further differentiation of the epithelium. Cells were maintained under ALC for 2-3 weeks before experiments.

To test putative RNF5 inhibitors, compounds were added to the basolateral medium 24 hr prior to the experiments to achieve the required concentration. Control epithelia were treated with vehicle alone (DMSO).

METHOD DETAILS

Homology Modeling

Starting from the RNF5 sequence (Q99942) downloaded from the UniProt (The UniProt Consortium, 2017), the structure was built with the Prime software (Schrödinger Release 2016-3: Prime, Schrödinger, LLC, New York, NY, 2016) on the basis of the structures (PDB: 1JM7_A, 4A4B_A, 2Y1M_A, 2Y1N_A, 1FBV_A, 4A49_A, 3VGO_A, 2LDR_A, 2JMD_A, 4AYC_A, 2ECJ_A, 2ECI_A, 2XEU_A, 2YSL_A, 3NG2_A, 3HCT_A, 3HCU_A, 4AP4_A, 3HCS_A, 3LRQ_A, 2YSJ_A, 2ECN_A, 4AUQ_B, 3FL2_A, 2ECW_A, 4FWE_A, 2D8T_A, 2EA6_A, 2H0D_A, 2CKL_A, 2ECT_A, 3RPG_B, 2CT2_A, 2ECV_A, 3L11_A, 2KIZ_A), using ClustalW for sequence alignment and composite/chimera-based as the knowledge-based building method.

Molecular Dynamics

The model of RNF5 was optimized with the Protein Preparation Wizard (Schrödinger Release 2016-3: Protein Preparation Wizard, Schrödinger, LLC, New York, NY, 2016), and then subjected to molecular dynamics (MD) simulations.

We performed an exhaustive sampling of the orientations of groups where the H-bond network needs to be optimized. Finally, the protein structure was refined to relieve steric clashes with a restrained minimization with the OPLS2005 force field until a final RMSD of 0.30 Å with respect to the input protein coordinates.

An MD simulation of the resulting protein structure was performed using Desmond (Schrödinger Release 2016-3: Desmond Molecular Dynamics System, D. E. Shaw Research, New York, NY, 2016). The protein was neutralized using sodium counterions. The protein and the counterions were immersed in an orthorhombic periodic TIP4P water bath that extended about 10 Å in each direction. After an initial default relaxation protocol, an MD production run was performed for 250 ns with a time step of 2 fs.

Life Chemicals Database Preparation

The Life Chemicals (<http://www.lifechemicals.com>) database collected directly from the vendor was prepared with LigPrep (Schrödinger Release 2016-3: LigPrep, Schrödinger, LLC, New York, NY, 2016).

The 2D structures were converted into 3D structures and, for each entry, all stereoisomers were generated. The resulting molecules were submitted to Epik, and all the tautomers and ionization states at pH 7.0 ± 2.0 were calculated. Finally, we deleted duplicates, compounds with more than 2 chiral centers, Pan-Assay Interference Compounds (PAINS), compounds with Michael acceptor groups, and frequent hitters.

To enrich the database with potential Protein-Protein Interaction Inhibitors, it was filtered with the PPI-HitProfiler tool (Reynès et al., 2010) using the “soft” methods.

Virtual Screening by High-Throughput Docking

From the last 100 ns of MD simulations, 10 protein conformations were collected by clustering on the basis of the RMSD. For all the collected structures, the most druggable pocket was searched with SiteMap (Schrödinger Release 2016-3: SiteMap, Schrödinger, LLC, New York, NY, 2016). In this pocket, all the ligands from the Life Chemicals database (about 500K) were docked with the software Glide (Schrödinger Release 2016-3: Glide, Schrödinger, LLC, New York, NY, 2016) (SP) and the best 1000 top-scoring compounds for each selected protein conformation were stored. All the selected compounds (10,000) were further filtered. First, the binding modes were visually inspected and the compounds were discarded based on a visual inspection analysis. In particular, molecules that did not show any clear chemical interactions with the target were considered false positive. This step, which depends on the chemical intuition and experience of the user, can help addressing the well-known weakness of docking scoring functions. Then, duplicate compounds were eliminated and the remaining compounds were grouped into 1,000 chemical clusters on the basis of the MOLPRINT 2D fingerprints using Tanimoto distance. Finally, we selected one or two representative of each cluster (depending on the cluster size) ending up to a total of 1,623 compounds, which were eventually purchased.

Diversity Set Selection

As a first step, we removed from the Life Chemicals database the 1,623 compounds selected by the previous virtual screening campaign. Then, to increase chemical diversity of the final set of compounds to submit to biological testing, we identified further 1,000 molecules that spanned the entire descriptor space of the Life Chemical database. This step was carried out by means of the Canvans software (Schrödinger Release 2016-3: Canvas, Schrödinger, LLC, New York, NY, 2016) on the basis of the MOLPRINT 2D fingerprints, using “sphere” as the diversity selection method.

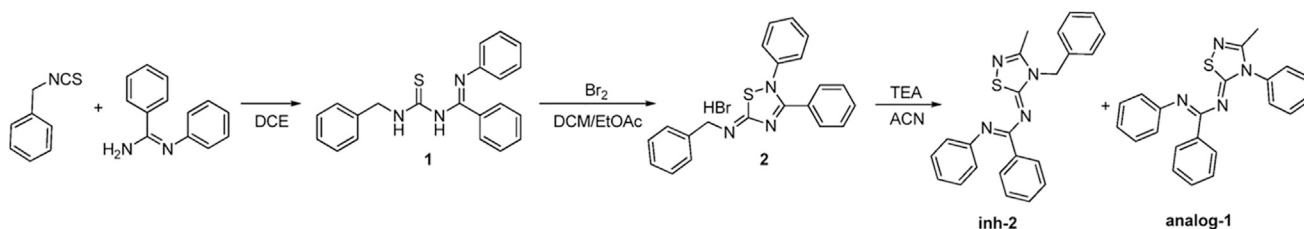
Compound Library Screening

Twenty-four hours after seeding on 96-well plates, CFBE410⁻ or FRT cells stably expressing F508del-CFTR and the HS-YFP were treated with test compounds at the desired concentration, one compound per well. Cells treated with vehicle alone (DMSO) and with corrector VX-809 (1 μM), respectively, served as negative and positive controls. In parallel, as an additional control, CFBE410⁻ cells were also reverse-transfected with siRNA targeting RNF5 (30 nM final concentration).

Synthesis of Compounds

Scheme 1 illustrates the synthetic route to **inh-2**. Reaction of N-phenylbenzamidine with benzyl isothiocyanate (both commercially available) afforded thiourea **1**, which underwent bromine oxidation yielding thiadiazolium salt **2**. The latter was treated with acetonitrile (ACN) in the presence of triethylamine (TEA), yielding 1,2,4-thiadiazolyliedene **inh-2** as the main product, and **analog-1** as by-product.

General experimental details. Reaction progress was monitored by TLC on pre-coated silica gel plates (Kieselgel 60 F254, Merck) and visualized by UV254 light. Flash column chromatography was performed on silica gel (particle size 40-63 μM, Merck). If required, solvents were distilled prior to use. All reagents were obtained from the commercial sources and used without further purification. When stated, reactions were carried out in an inert atmosphere. For simplicity, solvents and reagents are indicated as follows: acetonitrile (ACN), dichloromethane (DCM), diethyl ether (Et₂O), dimethylsulfoxide (DMSO), ethanol (EtOH), ethyl acetate (EtOAc), methanol (MeOH), triethylamine (TEA). Compounds were named using the naming algorithm developed by CambridgeSoft Corporation and used in Chem-BioDraw Ultra 15.0.



Scheme 1. Synthetic Route to inh-2

QC analysis of both compounds was performed by UPLC/MS on a Waters ACQUITY UPLC/MS system comprising a Single Quadrupole Detector (SQD) Mass Spectrometer equipped with an Electrospray Ionization interface and a Photodiode Array Detector. Electrospray ionization in positive and negative mode was applied in the mass scan range 100-500 Da. The PDA range was 210-400 nm. The separation was carried out on an ACQUITY UPLC BEH C18 column (100x2.1 mm ID, particle size 1.7 μ m) with a VanGuard BEH C18 pre-column (5x2.1 mm ID, particle size 1.7 μ m).

The mobile phase was 10 mM NH_4OAc in H_2O at pH 5 adjusted with AcOH (A) and 10 mM NH_4OAc in MeCN- H_2O (95:5) at pH 5 (B). A linear gradient was applied starting at 50% B (initial hold for 0.2 min) to 100% B in 6 min with a flow rate = 0.5 ml/min.

Accurate mass data of both compounds were acquired on a Waters Synapt G2 mass spectrometer, coupled to the same chromatographic separation described above. High-resolution mass spectra were acquired in positive ion mode and recalibrated in real time using leucine enkephalin (2 ng/ml in water/ACN) as reference compound. NMR spectra of both compounds were acquired on either a Bruker Avance III 400 MHz spectrometer equipped with a Broad Band Inverse probe (BBI) at 300.0 K, using 150 μ L of 10 mM DMSO- d_6 solutions, into 3 mm disposable tubes, or using a Varian Gemini at 400 MHz and 100 MHz, respectively. Chemical shifts (δ H) were reported relative to TMS as the internal standard. The impurity identity was confirmed by superimposing the ^1H NMR spectrum with that of synthesized compounds, whose structure had previously been assigned in 2D experiments, acquired as follows: ^1H - ^1H COSY (COrelation Spectroscopy): 4 transients, 2048 data points, 128 increments, ^1H - ^{13}C HSQC (multiplicity edited Heteronuclear Single Quantum Coherence): 8 transients, 1024 data points, 256 increments.

Synthetic Procedures to Obtain Compounds inh-2, analog-1, and Intermediates 1-2

(1E,NZ)-N-(4-benzyl-3-methyl-1,2,4-thiadiazol-5(4H)-ylidene)-N'-phenylbenzimidamide **inh-2** and (1E,NZ)-N-(3-methyl-4-phenyl-1,2,4-thiadiazol-5(4H)-ylidene)-N'-phenylbenzimidamide **analog-1**.

To a suspension of thiadiazolium bromide salt **2** (100 mg, 0.23 mmol, 1 equiv) in ACN (2 mL), TEA (99 μ L, 0.71 mmol, 3 equiv) was added. The mixture became a clear solution, which was refluxed for 30 min, then quenched with ice. The mixture was extracted with DCM, washed with water, dried over Na_2SO_4 , and the solvent evaporated in vacuum. The crude product was purified via flash silica gel column chromatography (petroleum ether/EtOAc in 95/5 ratio), then washed with pentane and filtered, to give a mixture (45 mg, 51%) of inh-2 and analog-1 as pale-yellow powder, which was further purified by preparative HPLC (see below).

(E)-N-(benzylcarbamothioyl)-N'-phenylbenzimidamide **1**. A mixture of N-phenylbenzimidamide (1.18 g, 6 mmol, 1 equiv) and benzyl isothiocyanate (795 μ L, 6 mmol, 1 equiv) in 1,2-dichloroethane dry (10 mL) was heated at 55°C for 16 h, then cooled to room temperature, and the solvent was evaporated. The resulting residue was purified via flash silica gel column chromatography (petroleum ether/EtOAc in 80/20 ratio) to give **1** as an off-white solid (830 mg, 40% yield). ^1H NMR (400 MHz, Chloroform- d) δ 12.37 (s, 1H), 8.05 (s, 1H), 7.44 – 7.26 (m, 7H), 7.25 – 7.18 (m, 3H), 7.09 (t, J = 7.9 Hz, 2H), 6.98 – 6.88 (m, 1H), 6.67 – 6.53 (m, 2H), 4.96 (d, J = 5.3 Hz, 2H) ppm. MS (ES^+) 368 (345 + Na^+) (ES^-) 344 (345 – H^+)

(Z)-N-(2,3-diphenyl-1,2,4-thiadiazol-5(2H)-ylidene)-1-phenylmethanamine hydrobromide **2**. To a solution of thiourea **1** (460 mg, 1.30 mmol, 1 equiv) in a mixture of DCM/EtOAc (4/5.2 mL), a 0.5 M solution of bromine (133 μ L, 2.60 mmol, 2 equiv) in EtOAc was added dropwise at room temperature. The thiadiazole hydrobromide salt started to precipitate during the addition. Petroleum ether was added, and the mixture was left to stand at 3°C for 12 h, then filtered, washed with additional petroleum ether, and dried in vacuum to afford **2** as a yellow solid (491 mg, 89%). ^1H NMR (400 MHz, DMSO- d_6) δ 10.12 (d, J = 6.0 Hz, 1H), 7.72 – 7.47 (m, 8H), 7.47 – 7.34 (m, 6H), 7.34 – 7.26 (m, 1H), 4.93 (d, J = 6.0 Hz, 2H) ppm. MS (ES^+): 344 (M^+ H^+).

Purification of inh-2 and analog-1

The purification by preparative HPLC/MS was performed on a Waters LC/MS Autopurification system comprising a 3100 Single Quadrupole Mass Spectrometer equipped with an Electrospray Ionization Interface and a 2998 Photodiode Array Detector. The HPLC system included a 2747 Sample Manager, 2545 Binary Gradient Module, System Fluidic Organizer, and 515 HPLC Pump. Electrospray ionization in positive and negative mode was used in the mass scan range 100-500 Da. The PDA range was 210-400 nm. The purification was performed on an XBridgeTM Prep C18 OBD column (100x19 mm ID, particle size 5 μ m) with an XBridgeTM Prep C18 (10x19 mm ID, particle size 5 μ m) Guard Cartridge. The mobile phase was H_2O (A) and MeCN (B). A linear gradient was applied starting at 70% B (initial hold for 0.5 min) to 90% B in 7 min with a flow rate = 20 ml/min.

NMR Purity Assessment and Structural Elucidation of inh-2 and analog-1

NMR purity was assessed with the PULCON (Pulse Length Based Concentration Determination) external standard procedure (Wider and Dreier, 2006), by comparing a signal of the molecule with the signal of a certified standard (Maleic Acid, Sigma Aldrich, NMR reference standard), acquired in an independent spectrum. Briefly, 16 transients were accumulated over a spectral width of 20.55 ppm (with the offset positioned at 6.175 ppm), after the 90° pulse optimization (Wu and Otting, 2005), at a fixed receiver gain (64), using 30 s of interpulse delay and no steady state scans.

The impurity identity was confirmed by superimposing the 1H NMR spectrum with that of synthesized compounds, whose structure had previously been assigned using 2D experiments, acquired as follows: 1H-1H COSY (COrrrelation Spectroscopy): 4 transients, 2048 data points, 128 increments, 1H-13C HSQC (multiplicity edited Heteronuclear Single Quantum Coherence): 8 transients, 1024 data points, 256 increments.

Final Purity and Chemical Structures Data for inh-2 and analog-1

inh-2: ¹H NMR (400 MHz, DMSO-*d*₆) δ 7.44 – 7.34 (m, 5H), 7.34 – 7.15 (m, 7H), 7.02 (d, *J* = 7.4 Hz, 1H), 6.76 (dt, *J* = 7.7, 1.1 Hz, 2H), 5.56 (s, 2H), 2.41 (s, 3H) ppm. ¹³C NMR (101 MHz, dmsO) δ 170.7, 158.5, 153.7, 146.8, 135.9, 134.7, 129.5, 129.2 (2C), 128.9 (2C), 128.9 (2C), 128.0 (2C), 127.8, 127.0 (2C), 123.0, 122.0 (2C), 48.5, 16.22 ppm. HPLC-MS (ESI, *m/z*) *R*_t = 3.29 min. Accurate mass 385.1500 *m/z* (mass accuracy 3.4 ppm for brute formula C₂₃H₂₀N₄S detected as (M+H)⁺). Purity evaluation by NMR: 92.2%

analog-1: ¹H NMR (400 MHz, DMSO-*d*₆) δ 7.69 – 7.50 (m, 5H), 7.32 – 7.15 (m, 7H), 7.01 (t, *J* = 7.4 Hz, 1H), 6.79 – 6.69 (m, 2H), 2.19 (s, 3H) ppm. ¹³C NMR (101 MHz, dmsO) δ 182.5, 159.1, 153.1, 147.0, 136.9, 135.0, 130.1 (2C), 129.9, 129.8, 129.5 (2C), 129.4 (2C), 128.6 (2C), 128.3 (2C), 123.5, 122.4 (2C), 17.3 ppm. HPLC-MS (ESI, *m/z*) *R*_t = 3.60 min. Accurate mass 371.1324 *m/z* (mass accuracy -1.6 ppm for brute formula C₂₂H₁₈N₄S detected as (M+H)⁺). Purity evaluation by NMR: 88.7%

Gene Silencing by siRNA Transfection

CFBE410⁻ cells expressing F508del-CFTR and the HS-YFP were reverse-transfected with 30 nM (final concentration) siRNAs (Stealth, Life Technologies) using lipofectamine 2000 as transfection agent. Twenty-four hours after transfection and plating, the medium was changed, and the cells were incubated at 37°C for an additional 24 h, prior to processing the cells for functional or biochemical assays.

Fluorescence Assay for CFTR

At the time of the assay, cells were washed with PBS containing (in mM) 137 NaCl, 2.7 KCl, 8.1 Na₂HPO₄, 1.5 KH₂PO₄, 1 CaCl₂, and 0.5 MgCl₂. Cells were then incubated for 25 min with 60 μl of PBS plus forskolin (20 μM) and VX-770 (1 μM) to maximally stimulate F508del-CFTR. Cells were then transferred to a microplate reader (FluoStar Galaxy; BMG Labtech, Offenburg, Germany) for CFTR activity determination. The plate reader was equipped with high-quality excitation (HQ500/20X: 500 ± 10 nm) and emission (HQ535/30M: 535 ± 15 nm) filters for YFP (Chroma Technology). Each assay comprised a continuous 14-s fluorescence reading, 2 s before and 12 s after injection of 165 μl of an iodide-containing solution (PBS with Cl⁻ replaced by I⁻; final I⁻ concentration 100 mM). Data were normalized to the initial background-subtracted fluorescence. To determine I⁻ influx rate, the final 11 s of the data for each well were fitted with an exponential function to extrapolate initial slope (dF/dt). Reproducibility of results was confirmed by performing three independent experiments.

Transepithelial Electrical Resistance and Potential Difference Measurements (TEER/PD)

Both primary bronchial and FRT cells were treated with compounds at the indicated concentrations for 24 hr at 37°C and 5% CO₂, before measuring the Transepithelial Electrical Resistance (TEER) and/or Potential Difference (DP). In all experiments, TEER and DP were evaluated with an epithelial voltohmmeter (EVOM1, World Precision Instruments).

For primary bronchial cells, we performed experiments in Coon's modified Ham's F-12 medium where NaHCO₃ was replaced with 20 mM Hepes. After incubation for 1 h with medium modified on both sides of permeable supports at 37°C, we measured TEER and DP in basal conditions. Then, we added 10 μM amiloride, a specific inhibitor of epithelial sodium channel (ENaC). We then added 20 μM forskolin (FSK) and 50 μM Genistein on the epithelium's apical side and 20 μM FSK on the baso-lateral side in order to activate CFTR channels. Finally, we added 30 μM PPQ102, a specific inhibitor of CFTR, on the epithelium's apical side. After each treatment, we waited 10 min at 37°C before recording measurements. Data are expressed as means ± SEM, *n* = 4 independent epithelia (biological replicates) per experiments. Reproducibility of results was confirmed by performing two independent experiments per patient.

For FRT cells, we performed experiments in a solution contained 130 mM NaCl, 2.7 mM KCl, 1.5 mM KH₂PO₄, 1 mM CaCl₂, 0.5 mM MgCl₂, 10mM Na-HEPES (pH 7.3), and 10mM glucose. We measured TEER in basal conditions with the same solution on both sides of permeable supports. Then, we added 20 μM forskolin (FSK) and 50 μM Genistein on the epithelium's apical side and 20 μM FSK on baso-lateral side in order to activate CFTR channels. Finally, we added 30 μM PPQ102, a specific inhibitor of CFTR, on the epithelium's apical side. After each treatment, we waited 10 min at 37°C before recording measurements. Data are expressed as means ± SEM, *n* = 3.

Short-Circuit Current Recordings

Snapwell inserts carrying differentiated bronchial epithelia were mounted in a vertical diffusion chamber, resembling a Ussing chamber with internal fluid circulation. Both apical and basolateral hemichambers were filled with 5 ml of a solution containing (in mM): 126

NaCl, 0.38 KH₂PO₄, 2.13 K₂HPO₄, 1 MgSO₄, 1 CaCl₂, 24 NaHCO₃, and 10 glucose. Both sides were continuously bubbled with a gas mixture containing 5% CO₂ - 95% air, and the temperature of the solution was kept at 37°C. The transepithelial voltage was short-circuited with a voltage-clamp (DVC-1000, World Precision Instruments) connected to the apical and basolateral chambers via Ag/AgCl electrodes and agar bridges (1 M KCl in 1% agar). The offset between voltage electrodes and the fluid resistance were adjusted to compensate the parameters before experiments. The short-circuit current was recorded with a PowerLab 4/25 (ADInstruments) analog-to-digital converter, connected to a Macintosh computer.

Data are expressed as means ± SEM, n = 5 independent epithelia (biological replicates) per experiments. Reproducibility of results was confirmed by performing two independent experiments. Statistical significance was tested by parametric ANOVA, followed by the Dunnett multiple comparisons test.

CFTR Immunoprecipitation (IP) Assay

CFBE41o⁻ cells stably expressing F508del-CFTR were grown to confluence on 60-mm diameter dishes and treated for 24 h with the indicated compounds in the absence or in the presence of MG-132 (10 μM) in the last 4 h. Then, cells were rinsed twice with ice-cold PBS without Ca²⁺/Mg²⁺ and then lysed with IP Lysis Buffer (#87788 Thermo Sci.) containing EDTA-free complete protease inhibitor (Roche), N-ethylmaleimide (5 mM) and MG-132 (20 μM). Nuclei were pelleted by centrifugation at 12,000 rpm at 4°C for 20 min. Supernatant protein concentration was calculated using the BCA assay (Euroclone) following the manufacturer's instructions. An aliquot of supernatant corresponding to 500 μg of protein was incubated for 1 hr with 2 μg/sample of mouse monoclonal anti-CFTR R24-1 antibody (R&D), rocking at room temperature. Antibody-antigen mixture was precipitated with 25 μl/sample of Pierce Protein A/G Magnetic Beads (Thermo Sci.) for 1 hr rocking at RT, following supplier instructions. Immunoprecipitated proteins were eluted from the resin under reducing conditions with 100 μl Laemli Sample Buffer 1X, at RT. Equal amount of IP products were analyzed by Western blotting (20 μl).

Western Blot

CFBE41o⁻ cells were grown to confluence on 60-mm diameter dishes, treated for 24 hr with the indicated compounds or silenced with the indicated siRNAs (30 nM final concentration) and lysed in RIPA buffer containing a complete protease inhibitor (Roche). Cell lysates were subjected to centrifugation at 12000 rpm at 4°C for 10 min. Supernatant protein concentration was calculated using the BCA assay (Euroclone) following the manufacturer's instructions. Equal amounts of protein (30 μg to detect LC3B and p62) were separated onto gradient (4-20% depending on target protein molecular weight) Criterion TGX Precast gels (Bio-rad laboratories Inc.), then transferred to nitrocellulose membrane with Trans-Blot Turbo system (Bio-rad Laboratories Inc.) and analyzed by Western blotting. Proteins were detected using antibodies indicated in the [STAR Methods](#) section. The proteins were then visualized by chemiluminescence using the SuperSignal West Femto Substrate (Thermo Scientific). Chemiluminescence was monitored using the Molecular Imager ChemiDoc XRS System. Images were analyzed with ImageJ software (National Institutes of Health). Bands were analyzed as Region-of-Interest (ROI), normalized against the GAPDH loading control. The molecular weight of the proteins (on the basis of the Precision Plus Protein WesternC Standards, Bio-rad Laboratories Inc.) and the lane density profiles of ubiquitylated CFTR were calculated using the band analysis program of the software Quantity one 4.6 of the Molecular Imager ChemiDoc XRS System. Data are presented as mean ± SEM of independent experiments.

To evaluate F508del-CFTR half-life, CFBE41o⁻ cells were plated and, after 24 hr, treated with the indicated compounds. The following day cells were treated with cycloheximide (CHX; 150 μg/ml) (SigmaAldrich). At different time point (0 - 2 - 4 - 6 hours), cells were then lysed in RIPA buffer 1X and subjected to SDS-PAGE as previously described. Reproducibility of results was confirmed by performing three independent experiments.

Proliferation Study

CFBE41o⁻ cells stably expressing F508del-CFTR and the HS-YFP were plated at low density (5,000 cell/well) on 96-well plates suitable for high-content imaging. After 6 hours, cells were treated with different concentrations of test compounds or vehicle alone (DMSO). Cell proliferation was monitored for 48 h using the Opera Phenix (PerkinElmer) high-content screening system. Alternatively, to monitor cytotoxic effect of high concentrations of test compounds, CFBE41o⁻ cells were plated (10,000 cell/well) and treated (after 6 hours) with test compounds or vehicle alone (DMSO). After 24 hours, cells were counterstained with Hoechst 33342 and propidium iodide to visualize total cells and apoptotic cells, respectively, and imaged by using the Opera Phenix (PerkinElmer) high-content screening system. Data are expressed as means ± SEM, n = 6. Reproducibility of results was confirmed by performing three independent experiments. Statistical significance was tested by parametric ANOVA, followed by the Dunnett multiple comparisons test.

MTT Tetrazolium Cell Viability Assay

CFBE41o⁻ cells were plated (10,000 cell/well) on 96-well plates. After 6 hours, cells were treated with different concentrations of test compounds or vehicle alone (DMSO). The following day, the 3-(4,5-dimethylthiazol-2-yl)-2,5-diphenyltetrazolium bromide (MTT) substrate was added to the medium at a final concentration of 0.5 mg/ml, and incubated for 3 hours at 37°C. Formazan production (proportional to the number of viable cells) was then quantified by recording changes in absorbance at 560 nm using a plate reader equipped for absorbance measurements (Victor3, Perkin Elmer).

In Vivo Ubiquitylation Assay

In vivo ubiquitylation assays were performed as previously described (Kuang et al., 2012). In brief, CFBE41o⁻ cells stably expressing F508del-CFTR were grown to confluence on 60-mm diameter dishes, treated for 24 hr with the indicated compounds or silenced with the indicated siRNAs (30 nM final concentration) and lysed in lysis buffer (2% SDS, 150 mM NaCl, 10 mM Tris-HCl pH 8.0) supplemented with 2 mM sodium orthovanadate, 50 mM sodium fluoride, and protease inhibitors (Complete EDTA-free, Roche). Lysates were then diluted 1:10 with dilution buffer (10 mM Tris-HCl pH 8.0, 150 mM NaCl, 2 mM EDTA, 1% Triton X-100). Diluted cell lysates were subjected to centrifugation at 14000 rpm at 4°C for 30 min. Supernatants were pre-cleared using protein A-G magnetic beads (Thermo Fisher) under rotation for 30 min and then immunoprecipitated using an anti-ATG4B antibody. Immunoprecipitants were subjected to SDS-PAGE for immunoblotting analysis. Detection of ubiquitin and target proteins was performed using the antibodies indicated in the STAR Methods section. Reproducibility of results was confirmed by performing three independent experiments.

Labeling of Autophagic Vacuoles with Monodansylcadaverine (MDC)

CFBE41o⁻ cells stably expressing F508del-CFTR and the HS-YFP were plated (50,000 cells/well) on good-quality clear-bottom 96-well black microplates suitable for high-content imaging. After 24 hr, cells were treated with test compounds or DMSO (as negative control). After 24 hr, cells were washed and incubated with 50 μM MDC (Sigma-Aldrich) in PBS at 37°C for 10 min (Biederbick et al., 1995). After incubation, cells were washed three times with PBS and immediately analyzed. High-content imaging and data analysis were performed using an Opera Phenix (PerkinElmer) high-content screening system. Wells were imaged in confocal mode, using a 40X water-immersion objective. MDC signal was laser-excited at 405 nm and the emission wavelengths were collected between 435 and 550 nm.

Data analysis of MDC spot number was performed using the Harmony software (ver 4.5) of the Opera Phenix high-content system.

Data are expressed as means ± SEM, n = 3 independent experiments. Statistical significance was tested by parametric ANOVA followed by the Dunnett multiple comparisons test (all groups against the control group).

Analysis of Actin Cytoskeleton

CFBE41o⁻ cells stably expressing F508del-CFTR and the HS-YFP were plated (50,000 cells/well) on good-quality clear-bottom 96-well black microplates suitable for high-content imaging. After 24 hr, cells were treated with test compounds or DMSO (as negative control). After additional 24 hr, cells were washed, formalin-fixed, and actin was labeled using phalloidin conjugated to Alexa Fluor 647. Cell nuclei were counterstained with Hoechst 33342. High-content imaging was performed using an Opera Phenix (PerkinElmer) high-content screening system. Wells were imaged in confocal mode, using a 40X water-immersion objective. Phalloidin signal was laser-excited at 640 nm and the emission wavelengths were collected between 650 and 760 nm. Excitation and emission wavelengths for visualization of Hoechst 33342 signal were 405 and between 435 and 480 nm, respectively.

Analysis of the signal texture was performed using the PhenoLogic machine-learning algorithm of the Harmony software (version 4.5) of the Opera Phenix high-content system. Analysis of signal texture was based on evaluation of Haralick and Gabor features, two subsets of well-known parameters (Haralick et al., 1973; Turner, 1986), and evaluation of SER (Spots, Edges, Ridges) features, developed by PerkinElmer and included in the Harmony software of Opera Phenix.

Scratch Wound Healing Assay

CFPAC-1 cells stably expressing the HS-YFP were plated (50,000 cells/well) on good-quality clear-bottom 96-well black microplates suitable for high-content imaging. After 24 hr, cells had reached 100% confluency. The cells were then pre-treated for 2 hr with mitomycin C (30 μM; Sigma-Aldrich) or DMSO. Cell monolayers in all wells were then scratched mechanically, using pipette tips mounted on a 12-channel pipette. After the scratch, wells were washed with PBS to remove detached cells and debris and fresh medium was added, containing test compounds (5 μM) or vehicle alone (DMSO; as negative control) in the absence (for cells pre-treated with DMSO) or presence of mitomycin C (30 μM; for cells pre-treated with this compound). For each condition, 32 individually scratched monolayers were assayed, and we performed three independent experiments. High-content imaging and data analysis for each well was performed using an Opera Phenix (PerkinElmer) high-content screening system. Wells were imaged using a 10X air objective.

YFP signal was laser-excited at 490-500 nm and the emission wavelengths were collected between 500 and 550 nm.

Data analysis of open area percentage was performed using the Harmony software (ver 4.5) of the Opera Phenix high-content system.

Data are expressed as means ± SEM, n = 32 independently scratched monolayers per experimental condition. Reproducibility of results was confirmed by performing three independent experiments. Statistical significance was tested by parametric ANOVA followed by the Dunnett multiple comparisons test (all groups against the control group).

QUANTIFICATION AND STATISTICAL ANALYSIS

We used the analysis of variance (ANOVA) followed by a post hoc test to avoid “multiple comparison errors” when comparing more than 2 groups. For normally distributed quantitative variables, a parametric ANOVA was performed. When the quantitative variables were skewed, the non-parametric ANOVA (Kruskal-Wallis test) was applied. The Kolmogorov-Smirnov test was used to evaluate the assumption of normality.

Statistical significance of the effect of single siRNA treatments on CFTR activity or expression in CFBE41o⁻ cells was tested by parametric one-way analysis of variance (ANOVA) followed by the Dunnett multiple comparisons test (all groups against the control group) as a post hoc test. For combinations of siRNAs against more than one target, we verified the statistical significance using ANOVA followed by the Tukey test (for multiple comparisons) as a post hoc test.

Normally distributed data are expressed as mean \pm SEM, while skewed distributed data are expressed as median (min-max), and significances are two-sided. Differences were considered statistically significant when $p < 0.05$.